nature microbiology

ARTICLES

https://doi.org/10.1038/s41564-019-0518-2

An RNA-centric dissection of host complexes controlling flavivirus infection

Yaw Shin Ooi[1,8], Karim Majzoub[1,2,8], Ryan A. Flynn[3,8*], Miguel A. Mata[1], Jonathan Diep[1], Jason Kenichi Li[4], Nicholas van Buuren[4], Neil Rumachik[3], Alex G. Johnson[5], Andreas S. Puschnik[1], Caleb D. Marceau[1], Luwanika Mlera[6], Jeffrey M. Grabowski[6], Karla Kirkegaard[4], Marshall E. Bloom[6], Peter Sarnow[1], Carolyn R. Bertozzi[3,7] and Jan E. Carette[1*]

Flaviviruses, including dengue virus (DENV) and Zika virus (ZIKV), cause severe human disease. Co-opting cellular factors for viral translation and viral genome replication at the endoplasmic reticulum is a shared replication strategy, despite different clinical outcomes. Although the protein products of these viruses have been studied in depth, how the RNA genomes operate inside human cells is poorly understood. Using comprehensive identification of RNA-binding proteins by mass spectrometry (ChIRP-MS), we took an RNA-centric viewpoint of flaviviral infection and identified several hundred proteins associated with both DENV and ZIKV genomic RNA in human cells. Genome-scale knockout screens assigned putative functional relevance to the RNA–protein interactions observed by ChIRP-MS. The endoplasmic-reticulum-localized RNA-binding proteins vigilin and ribosome-binding protein 1 directly bound viral RNA and each acted at distinct stages in the life cycle of flaviviruses. Thus, this versatile strategy can elucidate features of human biology that control the pathogenesis of clinically relevant viruses.

Mosquito-borne flaviviruses such as dengue virus (DENV) and Zika virus (ZIKV) severely impact global health with an estimated 100 million individuals suffering from DENV-induced illness alone[1,2]. Gaining insights into the mechanisms by which flaviviruses exploit their host environment to promote viral propagation could yield targets for host-directed therapies to combat infections[3,4]. Flaviviruses enter cells through receptor-mediated endocytosis and following membrane fusion the viral genomes are released into the cytoplasm. The approximately 11 kilobase (kb) flavivirus genomic RNA encodes a single viral polyprotein, which is subsequently cleaved into mature structural and non-structural proteins. Biogenesis of the flaviviral proteins, which occurs at endoplasmic reticulum (ER) membranes, is not trivial due to the size of the polyprotein (approximately 3,300 amino acids), the occurrence of multiple transmembrane regions, and the co-translational cleavage by viral and cellular proteases. After an initial round of translation, the RNA serves as a template for RNA replication, which occurs in close association to the ER membrane and primarily requires the NS5 RNA-dependent polymerase and NS3 helicase with involvement of other non-structural proteins and poorly defined host factors. The viral RNA–protein interactions are essential for recruiting and retaining the RNA at these ER sites, and for mobilizing the cellular factors required for translation, replication and packaging[5–7]. Although the viral RNA (vRNA) constitutes a central molecular hub during flavivirus infection, the precise molecular details have yet to be unravelled[8]. A global survey of cellular RNA-binding proteins (RBPs) interacting with vRNAs during infection would provide molecular insights into the composition and function of the ribonucleoprotein machines that drive vRNA translation and replication.

Results

Unbiased discovery of the flaviviral genomic RNA–protein interactome. To define the compendium of host proteins that associate with the positive-strand vRNA, we implemented comprehensive identification of RBPs by mass spectrometry (ChIRP-MS)[9]. The human hepatoma cell line Huh7.5.1, which supports high levels of flaviviral replication, was infected with either DENV-2 or ZIKV at a multiplicity of infection (m.o.i.) of 0.1 for 48 h. The infected cells were subsequently crosslinked with formaldehyde to preserve the in-cell interactions between proteins and RNAs and stabilize the ribonucleoprotein complexes. Biotinylated oligonucleotides (Supplementary Table 1) were used to specifically enrich for DENV or ZIKV RNA and the recovered proteins were subjected to label-free quantitative liquid chromatography with tandem mass spectrometry (LC–MS/MS; Fig. 1a). We recovered roughly 50% of the vRNA across the full length of each vRNA, suggesting robust sampling of the total cellular vRNAs, while strongly depleting highly abundant host RNAs such as 7SK and ribosomal RNA, as shown by analysis of the quantitative PCR with reverse transcription (qRT–PCR; Supplementary Fig. 1a). The tiled probes were also able to capture full-length DENV-2 RNA from the total RNA of infected Huh7.5.1 cells while depleting all other cellular RNAs (Supplementary Fig. 1b,c). Together, these experiments provide strong evidence that ChIRP enrichment for DENV and ZIKV RNA is specific and efficient.

Investigation of the ChIRP-MS revealed extensive coverage of both DENV and ZIKV polyproteins including the structural (C, PrM and E) and non-structural (NS1–NS5) viral proteins (Fig. 1b–d). Analysis of the peptide coverage per protein length revealed that the viral NS3 and NS5 were the most abundant recovered proteins

[1]Department of Microbiology and Immunology, Stanford University, Stanford, CA, USA. [2]INSERM U1110, Institute of Viral and Liver Diseases, University of Strasbourg, Strasbourg, France. [3]Department of Chemistry, Stanford University, Stanford, CA, USA. [4]Department of Genetics, Stanford University, Stanford, CA, USA. [5]Department of Chemical and Systems Biology, Stanford University, Stanford, CA, USA. [6]Biology of Vector-Borne Viruses Section, Rocky Mountain Laboratories, NIAID/NIH, Hamilton, MT, USA. [7]Howard Hughes Medical Institute, Stanford University, Stanford, CA, USA. [8]These authors contributed equally: Yaw Shin Ooi, Karim Majzoub, Ryan A. Flynn. *e-mail: raflynn@stanford.edu; carette@stanford.edu

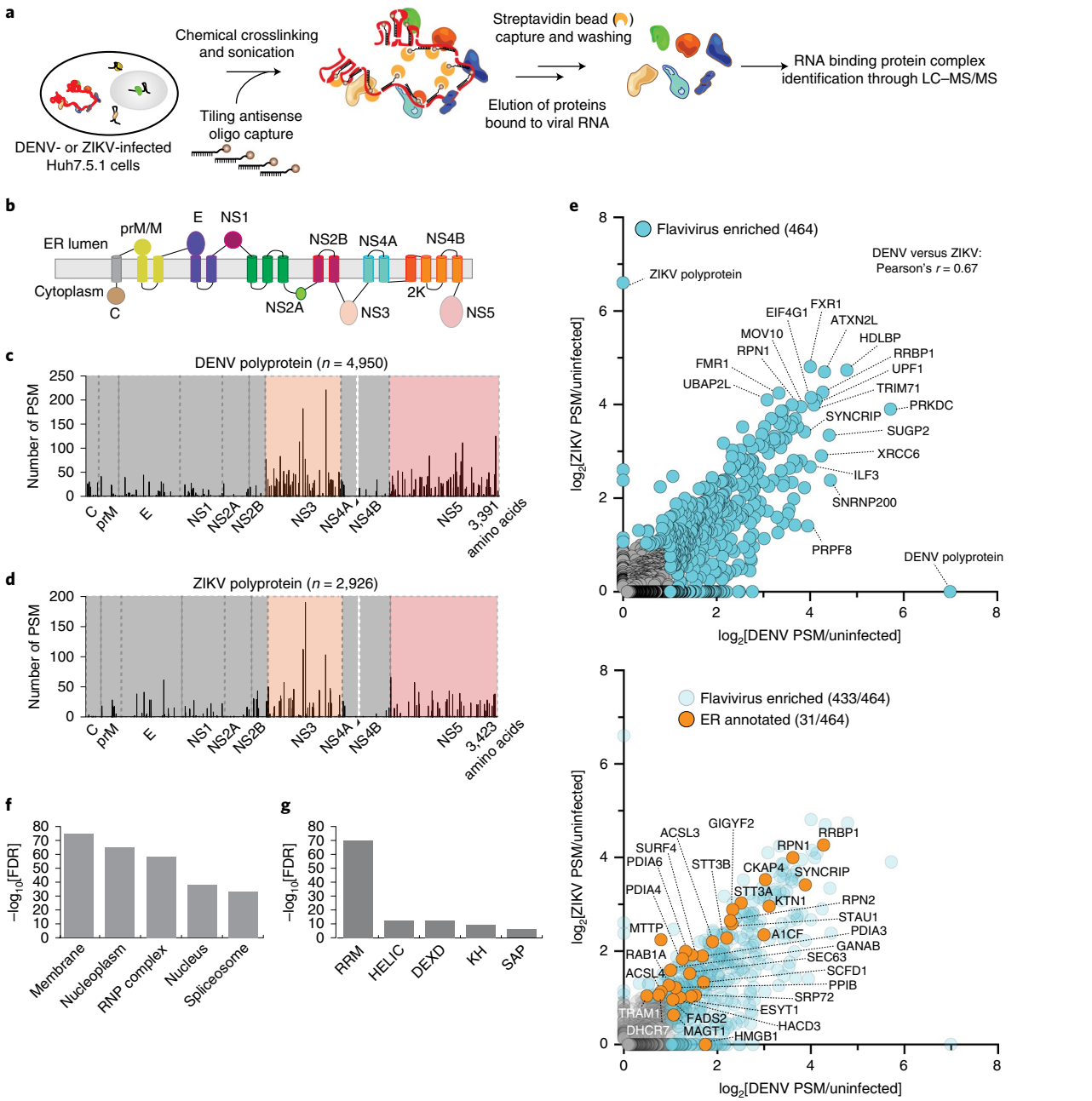

Fig. 1 | ChIRP-MS reveals the protein interactome of the DENV and ZIKV RNA genomes. a, Outline of the ChIRP-MS method. Uninfected and DENV- or ZIKV-infected Huh7.5.1 cells were formaldehyde crosslinked and solubilized by sonication. The target vRNA was pulled down by biotinylated antisense oligonucleotides, and the associated proteins were eluted and subjected to LC–MS/MS. **b**, Cartoon of the topology of the flaviviral polyprotein inserted in the ER membrane. **c**,**d**, Peptide-spectrum matches (PSM) the DENV (**c**) and ZIKV (**d**) genome with the corresponding mass-spectrometry spectral counts determined by ChIRP-MS. **e**, Scatter plots depicting the enrichment ratio of the host proteins identified by ChIRP-MS with DENV and ZIKV RNA over the uninfected background. A total number of 464 enriched proteins were identified for DENV and ZIKV, and several of the most enriched hits are indicated (top). Of the 464 enriched proteins, 31 are ER-annotated proteins and the remaining 433 proteins are implicated in other non-ER subcellular localizations (bottom). ChIRP-MS was performed in triplicate for each virus and the *x* and *y* axes represent the mean of the PSM-score enrichment over background for DENV and ZIKV, respectively. A full list of the enriched proteins is presented in Supplementary Table 2. **f**, Gene Ontology cellular-component analysis of the high-confidence host factors enriched by ChIRP-MS. **g**, Gene Ontology protein-domain analysis of the high-confidence host factors enriched by ChIRP-MS. **f**,**g**, The FDR calculation was performed using the Benjamini–Hochberg method on the combined ChIRP-MS enriched hits ($n=1$ merged dataset). PSM, peptide spectrum match; RNP, ribonucleoprotein.

(Supplementary Fig. 1d), which is consistent with these being RBPs that directly bind the flaviviral RNA. Our results are thus in line with ChIRP-MS enriching most strongly for RBPs but also for proteins present in functionally relevant RNA–protein complexes that do not directly interact with the RNA[10].

In addition to the virally encoded polyproteins, we identified 464 high-confidence hits from the human proteome that were specifically and reproducibly associated with DENV or ZIKV vRNA (false-discovery rate (FDR) < 0.01, SAINT score >0.99 and enrichment >2 fold over the uninfected control ChIRP-MS; Fig. 1e,

Supplementary Table 2 and Methods). The ChIRP-MS was highly consistent across the biological triplicates, confirming a strong intra-probe set reproducibility (Supplementary Fig. 1e,f). The enrichment of specific host factors recovered with DENV or ZIKV RNA were positively correlated (Pearson's $r=0.67$; Fig. 1e). RNA-binding proteins previously implicated in the antiviral response against DENV infection—including MOV10 (ref. [11]), YBX1 (ref. [12]) and ADAR[13]—as well as proteins with pro-viral functions, such as SND1 (ref. [14]), were among the highest-scoring candidates. Gene Ontology annotation revealed the strongest enrichment for the membrane component of cells (Fig. 1f). Protein-domain analysis of the hits was enriched for RNA-binding domains and the majority of the hits (approximately 75%) overlapped with a comprehensive list of mammalian RBPs[15] (Fig. 1g and Supplementary Table 2). Given the role of the ER membrane in flaviviral translation and the Gene Ontology enrichment, we examined ER-localized proteins in the ChIRP-MS data. The ER-localized proteins were enriched with high statistical significance ($P<0.0001$, Fischer's exact test) in the ChIRP-MS dataset (31/464) when compared with the fraction of ER-localized proteins expressed in Huh7.5.1 cells (421/18,199; Methods and Supplementary Tables 3,4). These data reinforce the idea that ChIRP-MS retrieves RBPs that associate with flaviviral RNA and that several of these are ER-proteins.

To determine the specificity of the RBPs for flaviviruses, we performed ChIRP-MS on an unrelated single-stranded RNA virus from the picornavirus family (rhinovirus (RV), strain RV-B14). We recovered 350 host proteins associated with rhinovirus RNA (Supplementary Table 5). A comparison between the host proteins associated with DENV or ZIKV and RV-B14 vRNA resulted in a weaker pairwise correlation (Supplementary Fig. 2a,b; Pearson's $r=0.40$ and 0.13, respectively) than between the two flaviviruses. Further, RV did not statistically enrich for ER-annotated factors (5/350 hits; Supplementary Fig. 2c and Supplementary Table 3), underscoring the important role the ER membrane plays in flaviviral biology. Thus, the DENV and ZIKV ChIRP-MS experiments provide a valuable resource of host factors that associate with flaviviral positive-strand RNA.

Genome-wide knockout screens reveal functional ChIRP-MS host factors. We and others have previously reported genome-wide knockout (KO) screens for DENV-2 (type strain 16681), ZIKV (African type strain MR766) and West Nile virus[16–19]. Here, we provide a higher granularity view to these studies by interrogating multiple serotypes and clinical isolates. We performed four clustered regularly interspaced short palindromic repeats (CRISPR)–CRISPR associated protein 9 (Cas9) screens in Huh7.5.1 cells by infecting them with four recently isolated and low-passaged DENV serotypes (that is, 1, 2, 3, and 4). For ZIKV, we performed haploid genetic screens utilizing three ZIKV strains isolated during recent epidemics in French Polynesia (FP/13), Puerto Rico (PRVABC59) and Colombia (FLR). The screen results were consistent and reproducible across the DENV serotypes and ZIKV strains (Supplementary Table 6). We merged the enrichment scores of the respective DENV (Fig. 2a) and ZIKV (Supplementary Fig. 3a) screens to obtain core sets of genes critical for flavivirus infection. Most of the identified host factors and pathways were related to the biogenesis of ER-targeted proteins and were common between DENV and ZIKV (Supplementary Fig. 3b,c and Supplementary Table 6). Collectively, these data represent a saturating analysis of host factors through seven genome-wide KO screens and highlight the importance of specific intracellular ER-associated protein complexes for DENV and ZIKV infection.

Because the DENV forward genetic screens and the ChIRP-MS were performed in the same Huh7.5.1 cell line, we compared these orthogonal techniques. Intersection of the top-200 hits from the DENV KO screens with the ChIRP-MS resulted in ten co-occurring proteins (Fig. 2b and Supplementary Table 6). Several subunits of the OST complex (STT3A, STT3B, RPN2 and MAGT1) were top hits in this dataset, both associating with the vRNA and of central importance for viral replication[16] (Fig. 2b). ASCC3 and SND1 were previously described to be important as a regulator of the cellular transcriptional response to flavivirus infection and as directly binding to vRNA, respectively[14,20]. Finally, two factors, vigilin and ribosome-binding protein 1 (RRBP1), that have not been previously linked to flavivirus infection stood out as among the most enriched in the ChIRP-MS (Supplementary Table 2 and Fig. 2b). We therefore focused on characterizing the molecular properties of these RBPs as well as defining the stages of the flaviviral life cycle at which these RBPs act.

To assess the impact of RRBP1 and vigilin on flaviviral infections, we generated isogenic KO lines (RRBP1-KO and vigilin-KO) in Huh7.5.1 cells (Fig. 2c). We then challenged RRBP1-KO and vigilin-KO cells with DENV, ZIKV and Powassan virus (POWV)—all of which belong to the flavivirus genus—or Chikungunya virus (CHIKV), an alphavirus. The vRNA loads were significantly reduced in the KO cells for most of the tested flaviviruses but the RNA levels of CHIKV were unaffected (Fig. 2d,e). The reduction of ZIKV infectivity in the KO cells was further validated using a luciferase-expressing ZIKV (ZIKV-Luc; Supplementary Fig. 3d). Thus, RRBP1 and vigilin are broadly required for members of the mosquito-borne (DENV and ZIKV) and tick-borne (POWV) flaviviruses but not for the unrelated arbovirus CHIKV. The abundance of viral proteins (for example, prM and NS3) was noticeably decreased in RRBP1-KO and vigilin-KO cells (Fig. 2f). The absence of RRBP1 and vigilin also led to a significant decrease in the production of infectious progeny virions (Fig. 2g). These results solidified RRBP1 and vigilin as host factors that promote flavivirus infections.

RRBP1 and vigilin interact at the ER. RRBP1/p180 is a highly expressed RBP anchored to the ER via a N-terminal transmembrane domain that can act as a messenger RNA receptor at the ER[21]. Vigilin promotes the translation of a subset of secretory mRNAs at the ER but, in contrast to RRBP1, lacks a transmembrane domain to anchor it to the ER[22]. Confocal microscopy revealed that both RRBP1 and vigilin co-localized with ER–green fluorescent protein (GFP), a previously reported ER marker[23], with RRBP1 exhibiting a slightly higher correlation than vigilin (0.69 and 0.60, respectively; Fig. 3a and Supplementary Fig. 4a). To assess the association with ER membranes more directly, we used a subcellular fractionation assay, which relies on a mild digitonin lysis to separate ER membranes from the cytosolic contents[24]. RRBP1 exclusively co-fractionated with the ER fraction, whereas vigilin was found in both the ER and cytosolic fractions (Fig. 3b). To test whether RRBP1 and vigilin associate with each other, we performed co-immunoprecipitation (co-IP) experiments. We found that vigilin co-immunoprecipitated with RRBP1 in uninfected and DENV-infected cells (Fig. 3c and Supplementary Fig. 4b). Treatment with RNase A markedly reduced the co-recovery of vigilin with RRBP1, suggesting that this interaction was RNA dependent (Fig. 3c and Supplementary Fig. 4b). Finally, during infection with DENV and ZIKV, both proteins co-localized with positive-stranded vRNA (Fig. 3d,e and Supplementary Fig. 4c,d). Together, our data indicate that RRBP1 and vigilin interact in an RNA-dependent manner at the ER close to the positive-stranded vRNA.

Global characterization of RNAs associated with RRBP1 and vigilin. To examine the interaction of RRBP1 and vigilin with viral and cellular RNA during infection, we performed infrared crosslinking and immunoprecipitation (irCLIP)[25] on uninfected and virus-infected cells. Primary antibodies targeting RRBP1 and vigilin generated an irCLIP RNAse-sensitive signal that was specific to their respective RBPs (Supplementary Fig. 5a,b). Further, mass-spectrometry

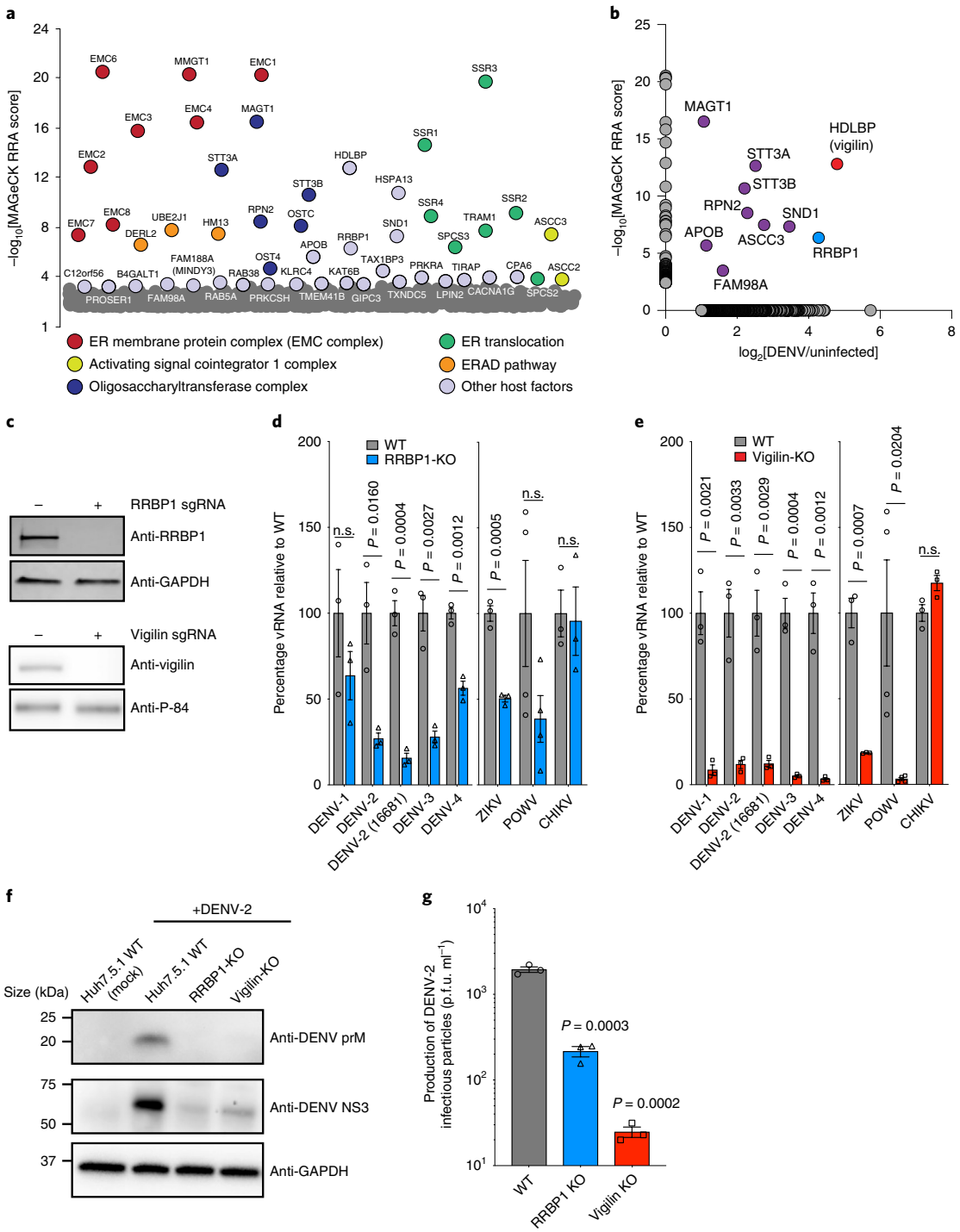

Fig. 2 | Intersection of ChIRP-MS with genome-wide CRISPR screens nominates functionally relevant pro-viral host proteins. a, Genome-scale CRISPR KO screens of all four DENV serotypes (DENV-1^{276RKI}, DENV-2^{429557}, DENV-3$^{Philippines/H871856}$ and DENV-4$^{BC287/97}$) in Huh7.5.1 cells. The genetic screens were independently performed for each serotype, analysed with MAGeCK and combined to obtain the robust rank aggregation (RRA) significance scores (*y* axis). The 50 most-enriched genes were coloured and grouped by function. **b**, Scatter plot depicting the enrichment scores of high-confidence ChIRP-MS DENV hits (*x* axis) and the 200 top-scoring hits from DENV CRISPR genetic screens (*y* axis). Common hits shared by both the DENV genetic screens and DENV ChIRP-MS are indicated in red (vigilin), blue (RRBP1) and purple (others). **c**, Western blot analysis of WT and clonal RRBP1-KO (top) or vigilin-KO (bottom) Huh7.5.1 cells. Representative western blot of $n = 2$ biologically independent replicates showing similar results. **d**, Analysis by qRT–PCR of WT and RRBP1-KO cells infected with DENV (48 h.p.i.; m.o.i. of 0.1), ZIKV^{PRVABC59} (48 h.p.i.; m.o.i. of 0.1), POWV^{LB} (48 h.p.i.; m.o.i. of 0.1) or CHIKV$^{181/25}$ (24 h.p.i.; m.o.i. of 0.01). **e**, Analysis by qRT–PCR of WT and vigilin-KO cells infected as in **d**. The WT datasets for POWV in **d**,**e** were derived from the same experiments. **f**, Western blot analysis of the cell lysates of DENV-2^{429557}-infected (72 h.p.i.; m.o.i. of 0.1) WT, RRBP1-KO and vigilin-KO Huh7.5.1 cells probed with antibodies to DENV prM and NS3. Representative western blot of $n = 4$ biologically independent replicates showing similar results. **g**, Titres of the infectious particles produced from WT, RRBP1-KO and vigilin-KO Huh7.5.1 cells infected with DENV-2^{429557} for 72 h at an m.o.i. of 0.1. **d**,**e**,**g**, The data represent the mean ± s.e.m. of $n = 3$ independent biological replicates, except POWV, where $n = 4$ independent biological replicates. All *P* values were determined by two-tailed, unpaired *t*-tests using GraphPad Prism; n.s., not significant.

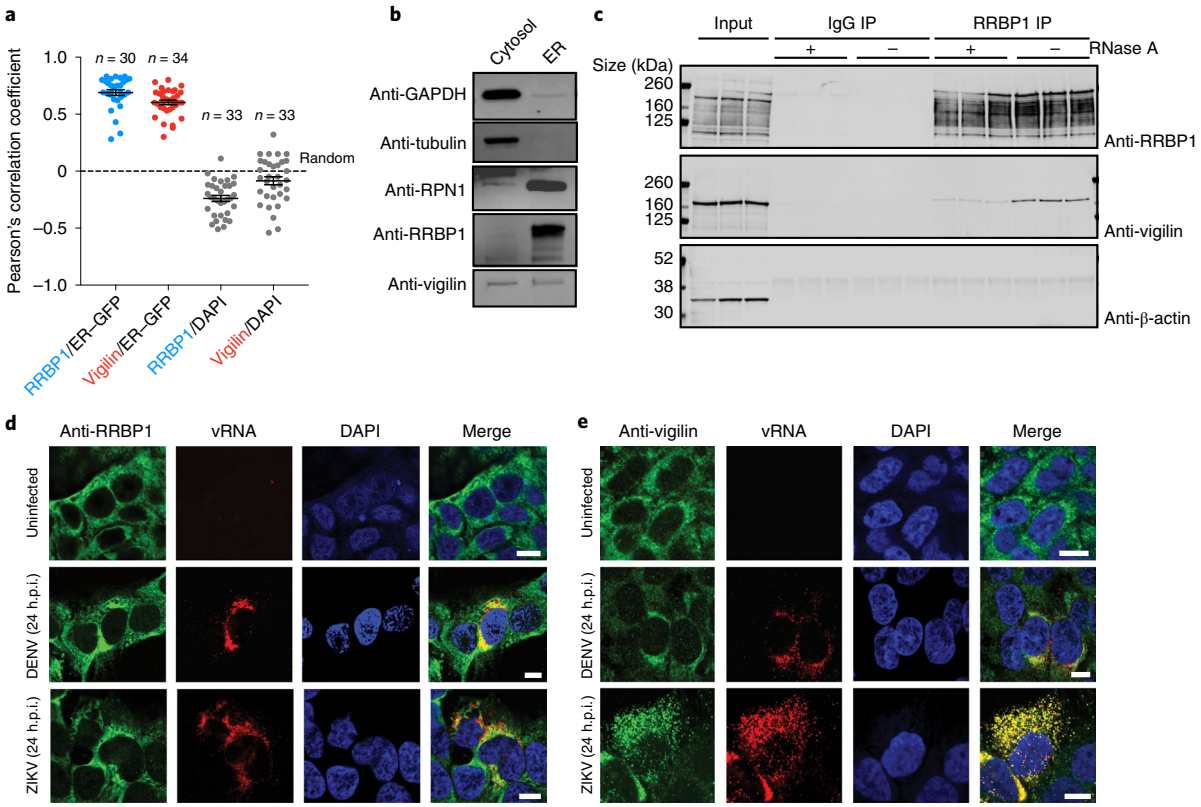

Fig. 3 | RRBP1 and vigilin interact at the ER. a, Single-cell quantification and correlation between RRBP1 or vigilin and the ER–GFP or DAPI immunofluorescence signals. The total numbers of cells that were randomly chosen for each analysis and the mean ± s.e.m. are indicated. **b**, Western blot analysis of the ER and cytosolic cell fractions probed with GAPDH or tubulin (cytosolic markers), RPN1 (ER marker), RRBP1 and vigilin antibodies. Representative western blot of $n = 3$ biologically independent replicates showing similar results. **c**, Western blot analysis of three independent co-IP experiments from uninfected Huh7.5.1 cells with RRBP1 as the bait showing similar results. The samples were treated with or without RNase A. **d**,**e**, Representative immunofluorescence of RRBP1 (**d**) and vigilin (**e**) co-stained with RNA fluorescent-in-situ-hybridization targeting of DENV or ZIKV positive-stranded RNA genomes. Representative images of $n = 2$ biologically independent replicates showing similar results. Scale bars, 10 μm. IP, immunoprecipitation.

analysis of proteins co-enriched with RRBP1 or vigilin irCLIP enrichments near their molecular weight confirmed their specificity (Supplementary Fig. 5c,d). Sequencing of the enriched RNAs revealed that RRBP1 had a preference for binding ribosomal RNA (66% rRNA) over messenger/non-coding RNA (33% mRNA/ncRNA; Fig. 4a), which is in line with its known direct association with ribosomes[26]. RRBP1 crosslinks to many sites across rRNAs with a strong peak in the 18S rRNA on helix 18 (H18) positioned near the mRNA entry channel[27] (Fig. 4b). In contrast to RRBP1, the vigilin reverse-transcriptase (RT) stops mapped mainly to mRNA/ncRNAs with only a minor contribution of rRNA (Fig. 4a). Interestingly, although vigilin has a more restricted rRNA-binding pattern, its major binding site is on H16 of the 18S rRNA, adjacent to the RRBP1-bound position at the mRNA entry channel (Fig. 4b).

Infection with DENV or ZIKV resulted in the appearance of reads derived from the viral positive-stranded genome for both RRBP1 and vigilin. The change in binding profile was especially apparent for vigilin, where 75% and 49% of all crosslinks mapped to the vRNA of DENV and ZIKV, respectively (Fig. 4a). Globally, for both RRBP1 and vigilin, RT stops mapping the mRNAs were depleted in intronic regions, suggesting a preference for mature transcripts (Fig. 4c). Vigilin preferentially bound exonic regions, whereas RRBP1 binding was enriched for binding to exons as well as to the 5′ and 3′ untranslated regions (UTRs; Fig. 4c). For both RRBP1 and vigilin, Gene Ontology analysis of the bound mRNAs revealed terms related to membrane-bound and secreted proteins known to be highly expressed in hepatic cells (Supplementary Tables 7 and 8)[28,29]. For RRBP1, in the context of infection, there was weaker enrichment for membrane terms, whereas there was a gain of novel terms such as cytosol and ribosome, suggesting differential localization of these mRNAs following infection (Supplementary Fig. 5e). For vigilin, the enrichments were quite similar between infected and uninfected cells (Supplementary Fig. 5f).

We next visualized the RT stops mapping to DENV or ZIKV RNA. RRBP1 crosslinked across the full-length positive-strand vRNA with RT stops extending into the 5′ and 3′ UTRs (Fig. 4d and Supplementary Fig. 6a). In contrast, vigilin bound to the coding region but markedly fewer RT stops were observed in the 5′ and 3′ UTRs (Fig. 4d). This pattern was similar to what was observed with cellular mRNAs (Fig. 4c and Supplementary Fig. 6b,c) and is in line with the previously reported preference for binding to coding regions[22]. We observed rather uniform binding throughout the vRNA without apparent hotspots for both RBPs. On a per nucleotide basis, RRBP1 and vigilin binding was positively correlated on the DENV and ZIKV genomes ($r = 0.79$ and 0.84, respectively; Supplementary Tables 7 and 8) but did not correlate to complementary DNA truncations from RNA sequencing (RNA-seq) of the vRNA, which suggests that the irCLIP profiles are specific (Supplementary Tables 7 and 8). This broad 'coating' of the vRNA is reminiscent of how other RBPs, such as FMRP, bind actively translating mRNAs[30]. Together, the comparative RNA-binding profiles of RRBP1 and vigilin show that both proteins engage cellular rRNA and secretory mRNAs, with RRBP1 demonstrating a higher proportion of rRNA binding. During infection, both RBPs bind flavivirus

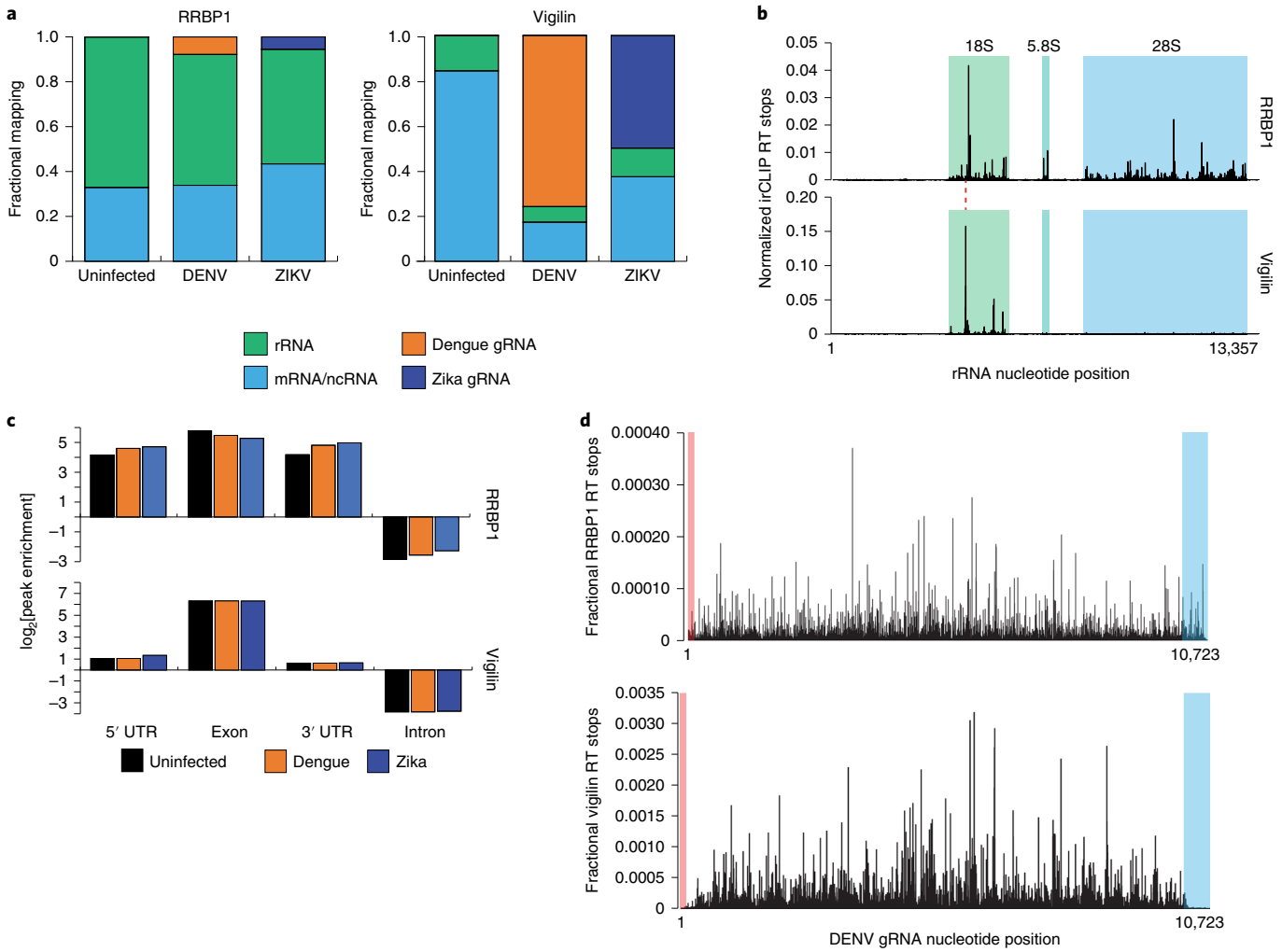

Fig. 4 | DENV and ZIKV co-opt the RNA-binding properties of RRBP1 and vigilin in human cells. a, RRBP1 (left) and vigilin (right) irCLIP RT-stop mapping statistics annotated to the human, and DENV and ZIKV genomes (gRNA) and the ribosomal RNAs (rRNA) from Huh7.5.1 cells infected with an m.o.i. of 0.1 for 48 h. **b**, Histogram of RT stops mapping to the rRNAs from the RRBP1 (top) and vigilin (bottom) irCLIP in uninfected Huh7.5.1 cells. The three cytosolic rRNAs are highlighted. The red dashed line denotes the strongest vigilin binding site, which is adjacent to that of RRBP1. **c**, Annotation of peaks called from the RRBP1 (top) and vigilin (bottom) irCLIP RT stops mapping to functional elements of human mRNAs including the 5′ UTR, exons, 3′ UTR and introns. The enrichment values were calculated based on the size of each function domain relative to the human genome. **d**, RRBP1 (top) and vigilin (bottom) irCLIP RT stops mapped at base resolution to the DENV genome. The RT stop intensity was normalized to the total number of unique reads mapping to the viral genome. The 5′ and 3′ UTR regions are highlighted in red and blue, respectively.

RNA and the majority of RT stops retrieved for vigilin are of flaviviral origin.

RRBP1 and vigilin are required for the optimal translation and replication of DENV. We further defined the step(s) at which the RBPs act in the viral life cycle by utilizing a luciferase-expressing DENV (DENV-Luc). First, we generated additional RRBP1 and vigilin clonal KO HEK293 cell lines to mitigate potential cell-type-specific effects (Supplementary Fig. 7a,b). RRBP1 and vigilin deficiency resulted in decreased luciferase expression throughout the infection cycle for DENV-Luc but not for the unrelated Coxsackievirus B3 virus expressing luciferase (Fig. 5a–d). Re-expression of RRBP1 and vigilin rescued, at least partially, the defect in flavivirus translation and replication, indicating that it is specific to the KO. To separate the translation and replication phase of the viral life cycle from the viral entry and uncoating steps, we transfected in vitro transcribed DENV replicon, in which the structural proteins are replaced with the *Renilla* luciferase gene. Compared with wild-type (WT) cells, the KO of both RBPs resulted in decreased luciferase expression throughout the time course (Fig. 5e,f). Because viral entry was bypassed in this experiment, these results suggest that RRBP1 and vigilin promote optimal viral translation and replication rather than viral entry.

Viral translation and replication are intricately linked: after the initial translation, viral non-structural proteins are produced that replicate genomic RNA, which in turn produces more mRNA templates resulting in increased translation. A larger contribution of initial translation is expected early in infection, whereas it is a combination of viral translation and replication at later time points. We performed DENV-Luc infections in the presence or absence of the DENV RNA replication inhibitor MK0608[31] to examine this in more detail and to assess the respective contributions of RRBP1 and vigilin to these phases. Control experiments confirmed that the luciferase signal at 8 h post-infection (h.p.i.) in the presence of MK0608 represents initial viral translation, whereas the bulk of the signal at 36 h.p.i. (in the absence of MK0608) is due to the subsequent RNA replication and translation (Supplementary Fig. 7c,d). Compared with the WT, RRBP1 deficiency resulted in an approximately

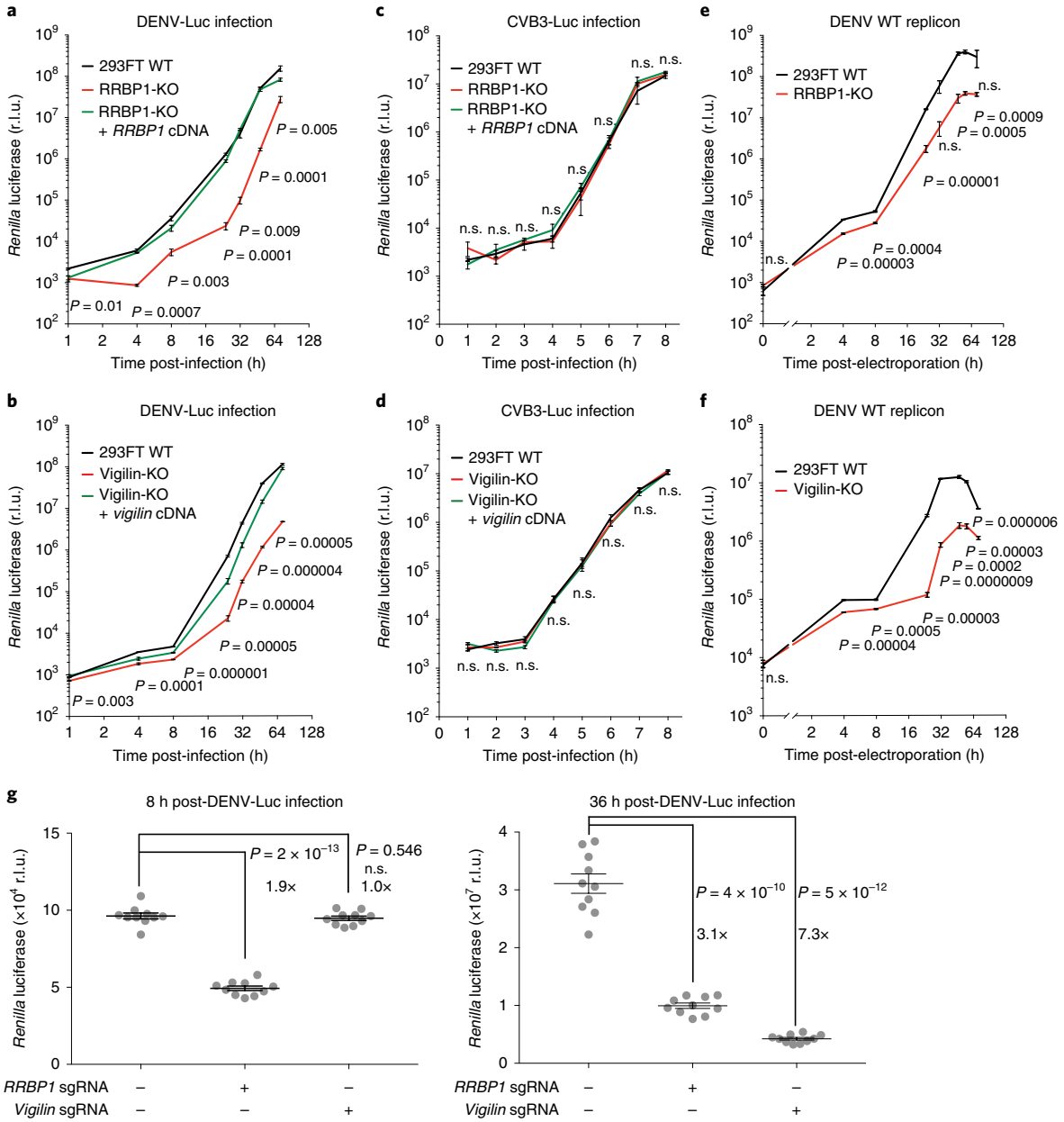

Fig. 5 | RRBP1 and vigilin modulate DENV translation and replication. a,**b**, Time-course DENV-Luc infection assays. WT, RRBP1-KO and RRBP1-KO + *RRBP1* cDNA rescue (**a**) or WT, vigilin-KO and vigilin-KO + *vigilin* cDNA rescue (**b**) HEK293FT cells were infected with DENV-Luc (m.o.i. of 0.01) and harvested at the indicated time points. Virus infectivity was then determined by measuring the *Renilla* luciferase expression of the infected cells. **c**,**d**, Time-course CVB3-Luc infection assays. WT, RRBP1-KO and RRBP1-KO + *RRBP1* cDNA rescue (**c**) or WT, vigilin-KO and vigilin-KO + *vigilin* cDNA rescue (**d**) HEK293FT cells were infected with CVB3-Luc (m.o.i. of 1) and harvested at the indicated time points. **e**,**f**, Luciferase expression of luciferase-encoding DENV replicon RNA in WT and RRBP1-KO (**e**) or WT and vigilin-KO (**f**) HEK293FT cells over the indicated time points post-electroporation of the replicon RNA. In **a**–**f**, the data in each panel represent the mean ± s.e.m. of $n = 3$ independent biological replicates. **g**, Luciferase expression 8 h (left) post-DENV-Luc (m.o.i. of 0.025) infection in the presence of the replication inhibitor MK0608 (50 μM final concentration) or 36 h (right) post-DENV-Luc infection in the presence of DMSO of WT, RRBP1-KO and vigilin-KO HEK293FT cells. The data in each panel represent the mean ± s.e.m. of $n = 10$ biologically independent infections. The fold change between datasets is indicated. All *P* values were determined by a two-tailed, unpaired *t*-test using GraphPad Prism. n.s., not significant; r.l.u., relative light units; sgRNA, single guide RNA.

twofold reduction of luciferase expression at 8 h.p.i., whereas vigilin deficiency did not decrease luciferase expression (Fig. 5g). However, vigilin-KO showed a more severe phenotype than RRBP1-KO at 36 h.p.i. (7× versus 3× reduction, respectively). We therefore conclude that the role of RRBP1 is more pronounced during the early stages of infection, whereas vigilin plays a more significant role at the later stages of infection.

Cellular RBPs contribute to DENV genomic RNA stability. We generated an isogenic cell line that is deficient in both RRBP1 and vigilin in Huh7.5.1 cells to further characterize the role of RRBP1 and vigilin (Fig. 6a). We observed a greater decrease in luciferase expression in the single RRBP1-KO cells compared with vigilin-KO cells early in infection and the reverse pattern later in infection with DENV-Luc, corroborating the RBP-KO viral phenotypes in HEK293

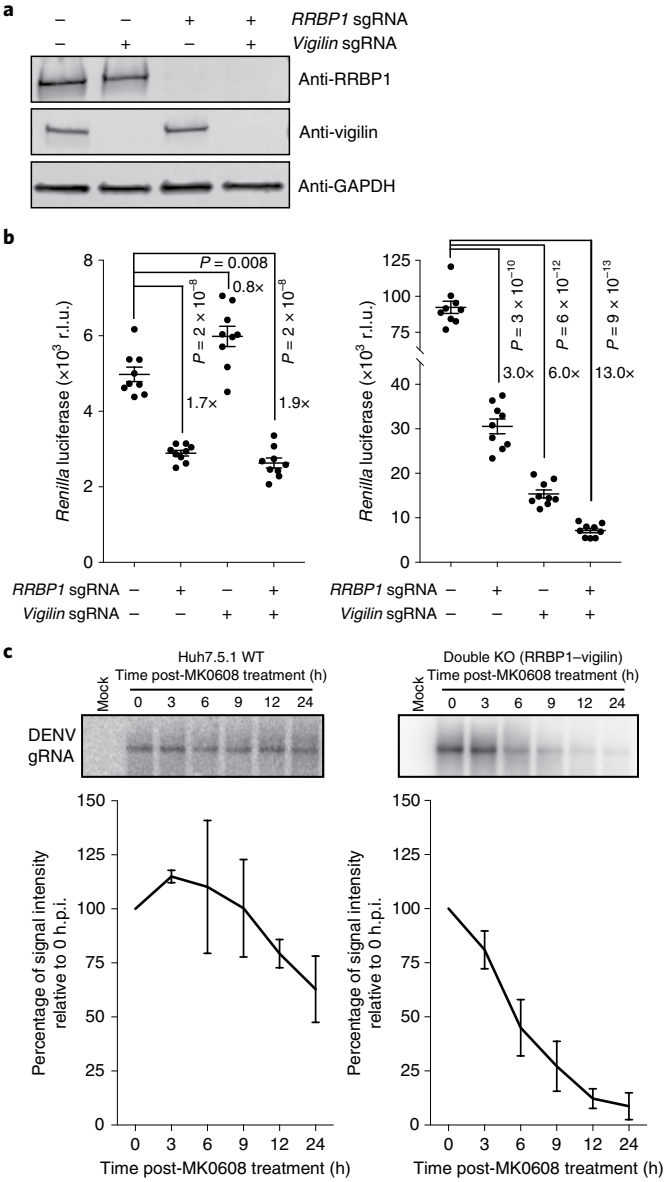

Fig. 6 | RRBP1 and vigilin promote DENV infection and vRNA stability. **a**, Western blot analysis of WT, vigilin-KO, RRBP1-KO and RRBP1-vigilin double-KO Huh7.5.1 cells. Representative western blot of $n = 2$ biologically independent replicates showing similar results. **b**, Luciferase expression at 8 h (left) and 24 h (right) following DENV-Luc infection (m.o.i. of 0.01) of WT, vigilin-KO, RRBP1-KO and RRBP1-vigilin double-KO Huh7.5.1 cells. The data in each panel represent the mean ± s.e.m. of $n = 9$ biologically independent infections. The *P* values were determined by two-tailed, unpaired *t*-tests using GraphPad Prism; n.s., non-significant. **c**, Northern blot analysis of DENV genomic RNA extracted from WT and RRBP1-vigilin double-KO Huh7.5.1 cells infected with DENV-2^{16681} (m.o.i. of 0.1) for 48 h, followed by treatment with MK0608 for the indicated time periods (top). Quantification of DENV genomic RNA (that is, northern-blot signal) from $n = 3$ independent experiments (the error bars are the s.e.m.) as a percentage relative to the time point 0 h after MK0608 treatment (bottom).

cells (Fig. 5g). The RRBP1-vigilin double-KO cells displayed an early defect comparable to RRBP1-KO cells and a late defect that was stronger than that observed for vigilin-KO cells (Fig. 6b), suggesting that both RBPs are required for optimal replication.

Our results combined with the known role of RRBP1 and vigilin in the translation of cellular mRNAs[32,33] suggest that the RBPs stimulate vRNA replication, at least partially, by promoting translation of the viral polyprotein. In addition to translation, both vigilin and RRBP1 can also act on the stability of their target mRNAs[34,35]. To assay for vRNA accumulation, we used MK0608 to inhibit viral replication and northern blotted against the DENV 3′ UTR, which allows the detection of vRNA decay (Fig. 6c). We observed that the accumulated DENV genomic RNA was relatively stable in the WT cells for up to 24 h following MK0608 treatment (Fig. 6c and Supplementary Fig. 8a). In contrast, the decay rate of the genomic RNA was accelerated in the absence of both RRBP1 and vigilin (Fig. 6c and Supplementary. 8b). Together, our data indicate that RRBP1 and vigilin promote optimal flavivirus infection and have roles in vRNA translation, replication and stability.

Discussion

Our results provide detailed insights into the molecular identity of the host machineries engaged by flaviviral RNA during infection. We have comprehensively mapped the interactions between the flaviviral RNA genome and the human cellular proteome during viral infection using ChIRP-MS. Intersecting this dataset with a core set of genes identified in our genetic screens using all serotypes of DENV and multiple strains of ZIKV (Supplementary Table 9) highlighted the importance of ER-localized RBPs for flavivirus infection. One example of an ER-localized RBP was RRBP1—which has a short luminal domain, a transmembrane domain, and a large domain facing the cytosol that is highly basic and contains a decapeptide tandem-repeat motif[36]. RRBP1 can act as a minor polysome receptor at the ER membrane[37] and it can also bind certain mRNAs in a ribosome-independent fashion[33]. Our data support these non-mutually exclusive views of RRBP1 function: the majority of RT stops identified from the RRBP1 irCLIP are indeed from the rRNA but nearly one-third of binding maps to mRNAs enriched for secretory protein transcripts (for example, APOB and AFP).

Vigilin is an evolutionarily conserved RBP that interacts with RNA through its KH domains. Although vigilin has been reported to be predominantly cytosolic, associating with free ribosomes[38], we detected a portion of vigilin in the ER fraction, thus corroborating previous observations of its association with ribosomes at the rough ER[39,40]. We found that vigilin directly binds to rRNA and is preferentially enriched for binding to a subset of cellular mRNAs that encode secretory proteins, indicating a potential role in translation. This is consistent with the emerging view of vigilin as a translational enhancer for a subset of mRNAs of the secretory pathway[22,41]. Our results indicate that DENV and ZIKV co-opt vigilin to promote infection.

Determining the protein interactome of RNA viruses has been a long-standing question of the field and is of interest to many laboratories. Two recent reports that utilized ultraviolet (UV) crosslinking and DENV RNA pulldown[42,43] found 12 and 93 host RBPs, respectively, that partially overlap with our ChIRP-MS data (Supplementary Table 10). We used ChIRP-MS as a robust platform to discover the protein interactomes of vRNA. We were careful to verify that the enrichment procedure would recover proteins binding across the entire length of the 11-kb viral genome as well as sample a majority of the vRNA from infected cells. These quality controls ensured that the resulting proteomic data would be as robust and complete as possible. Further, as a discovery tool, we opted for chemical crosslinking, which provides the context of RBP complexes associated with the target RNA.

Our study of the flavivirus RNA interactome is a valuable resource that provides an RNA-centric perspective on viral infection, complementing other large-scale approaches that map virus–host interactions. The strategy employed here, integrating RNA–protein interactome data with genome-scale KO screening, is a generalizable strategy for the study of the complex interactions of cellular proteins with other RNA viruses. Critically, rigorous

validation through isogenic KO of host factors and direct but unbiased assessment of their RNA interactomes with irCLIP provides a robust platform for the discovery of functional interactions. The approach emphasizes the RBPs that have a pro-viral role because of the design of the genetic screens but can readily be modified to include other large-scale approaches that identify proteins with antiviral activities[44].

Methods

Cell lines, reagents and generation of KO cells. HAP1 cells were derived from the near-haploid chronic myeloid leukaemia cell line KBM7 (ref. [45]). The HAP1 cells were cultured in IMDM medium supplemented with 10% heat-inactivated fetal bovine serum (HI-FBS), penicillin-streptomycin and L-glutamine. BHK-21 (ATCC), HEK293FT (Thermo Fischer Scientific), H1-HeLa cells (ATCC), Huh7.5.1 (gift from F. Chisari), RD (ATCC), BHK-21 (ATCC), Vero (ATCC) cells and their KO derivatives were cultured in DMEM media supplemented with 10% HI-FBS, 1×penicillin-streptomycin and 1×L-glutamine. C6/36 cells (ATCC) were purchased from the ATCC and cultured in Leibovitz's L-15 medium supplemented with penicillin-streptomycin, L-glutamine and 10% HI-FBS. Cycloheximide was purchased from Sigma-Aldrich. MK0608 (7-deaza-2'-*C*-methyladenosine) was purchased from Carbosynth.

A CRISPR–Cas9 strategy was employed to generate RRBP1- and vigilin-KO cell lines. CRISPR guide RNA sequences were designed using the Zhang lab CRISPR design tool (http://crispr.mit.edu) and the corresponding oligos were purchased from Integrated DNA Technologies. The oligos were cloned into the Cas9-expressing pX458 guide RNA plasmid (Addgene, cat. no. 48138) generated by the Zhang lab as previously described[16]. The cloning products were transfected into HEK293FT and Huh7.5.1 cells using Lipofectamine 3000 (Thermo Fisher Scientific) and subsequently single-cell sorted based on GFP expression into 96-well plates using a BD Influx cell sorter at the Stanford Shared FACS facility. Clonal cell lines were allowed to expand from a single cell and genomic DNA was isolated for sequencing-based genotyping of targeted alleles. For this, a 300–500 base-pair region that encompassed the guide-RNA-targeted site was amplified and the sequence of the PCR product was determined by Sanger sequencing. Subclones were chosen where all alleles were mutated with insertions or deletions that were not a factor of three. Knock-out subclones verified by genotyping were further confirmed by western blotting using antibodies against RRBP1 (Bethyl Laboratories, A303-996A) or vigilin (Bethyl Laboratories, A303-971A). The guide RNA primers are listed in Supplementary Table 1 and were cloned into the PX458 plasmid. RRBP1-vigilin double-KO Huh7.5.1 cell lines were generated by transfecting verified RRBP1-KO cells with the same PX458 plasmid containing vigilin guide RNA used earlier to knock out vigilin. Double-KO selection and characterization was performed by western-blot analysis on single-cell FACS-sorted clonal cells.

Viral strains, serotypes, reporter viruses and replicon. DENV-2 infectious clone 16681 was a gift from K. Kirkegaard (Stanford University). DENV-2 derived from infectious clone 16681 was a cell culture (HAP1 cells) adapted strain[16]. DENV-1^{276RKI} (isolated in 1997 from a human in India; cat. no. NR-3782), DENV-2^{429557} (isolated in 2005 in Mexico; cat. no. NR-12216), DENV-$3^{Philippines/H871856}$ (isolated in 1956 from human serum in the Philippines; cat. no. NR-80), DENV-$3^{VN/BID-V1009/2006}$ (isolated in 2006 from a human in Vietnam; cat. no. NR-44088) and DENV-$4^{BC287/97}$ (isolated in 1997 from a human in Mexico; cat. no. NR-3806), $ZIKV^{FLR}$ (isolated in 2015 from a human in Colombia; cat. no. NR-50183) and $ZIKV^{PRVABC59}$ (isolated in 2015 from a human in Puerto Rico; cat. no. NR-50240) were obtained from BEI resources (NIH, NIAID). $ZIKV^{H/PF/13}$ French Polynesia was provided by C. Blish (Stanford University). All DENV serotypes and ZIKV isolates were propagated in C6/36 cells. Infectious DENV and ZIKV particles were determined through titration using standard plaque assays in Huh7.5.1 cells, unless otherwise stated. The CHIKV (181/25 vaccine strain) was a gift from M. Kielian and was propagated and titred using a standard plaque assay in BHK-21 cells. The POWV LB-prototype-strain (originally obtained from R. Tesh, University of Texas Medical Branch)[46] stock was amplified and titred by a standard plaque assay in Vero cells.

The luciferase-encoding ZIKV infectious clone (ZIKV-Rluc) was provided by P.-Y. Shi, (UTMB) and the viral stock was generated in Vero cells as described[47]. The Coxsackievirus B3 Nancy strain that encodes *Renilla* luciferase (CVB3-Luc) was a gift from F. v. Kuppeveld and was propagated by transfection of the infectious clone pRLuc-53CB3/T7 into RD cells[48]. The titre of CVB3-Luc was determined by a standard plaque assay on H1-HeLa cells.

Construction of the pDENV-Luc infectious clone was performed as described[16]. The viral 5′ UTR was followed by a duplication of the first 104 nucleotides of the C coding region, which contains *cis*-acting elements required for replication (CAE). The CAE was fused to the *Renilla* luciferase coding region followed by the complete DENV open reading frame (ORF). A foot and mouth disease virus (FMDV) 2A sequence was introduced between the luciferase and the DENV structural proteins to provide co-translational cleavage and release of luciferase. The construct was based on pD2/IC-30P, which contains a full-length infectious clone encoding DENV-2^{16681} in which a Q399H mutation of the envelope protein (E) was introduced that enhanced viral infection in mammalian cells using the QuikChange site-directed mutagenesis kit (Agilent Technologies) and the primers listed in Supplementary Table 1. We gene-synthesized a fragment containing the T7-polymerase promoter sequence followed by the first 104 nucleotides of the C coding region in frame with *Renilla* luciferase and FMDV 2A. This fragment was PCR amplified, during which a SacI site at the 5′ end and a NheI site (present in the FMDV 2A sequence) at the 3′ end were introduced using the primers listed in Supplementary Table 1. To create an in-frame fusion of FMDV 2A with the DENV-ORF, a second DNA fragment was amplified using pD2/IC-30P as a template with primers (Supplementary Table 1) that introduced NheI and SphI restriction sites at the 5′ and 3′ ends, respectively. The two fragments were cut with the respective restriction enzymes and ligated into pD2/IC-30P cut with SacI and SphI to create pDENV-Luc. DENV-Luc virus was produced by cutting with XbaI to linearize the plasmid, transcribing pDENV-Luc in vitro using the MEGAscript T7 transcription kit (AM1334) and transfecting BHK-21 cells using Lipofectamine 2000. Filtered supernatant of transfected BHK-21 cells was used to infect Huh7.5.1 cells.

Construction of the DENV WT replicon was described previously[16] and was performed as per pDENV-Luc, except that the *Renilla* luciferase coding region was directly followed by the DENV ORF starting at the signal peptide preceding NS1, deleting the structural proteins. The construct was based on pD2/IC-30P, which contains a full-length infectious clone encoding DENV-2^{16681}. We gene-synthesized a fragment containing the T7-polymerase promoter sequence followed by the first 102 nucleotides of the C coding region in frame with *Renilla* luciferase and FMDV 2A followed by the DENV ORF starting at the signal peptide preceding NS1 up to an internal HpaI site. This fragment was released by SacI (preceding the T7 promoter) and HpaI, and cloned in pD2/IC-30P in a three-point ligation with KpnI/SacI and KpnI/HpaI fragments. The primer sequences are listed in Supplementary Table 1.

Constructs and packaging of lentivirus. To generate a lentiviral construct expressing GFP–RRBP1, the cDNA construct (provided by A. Palazzo, University of Toronto)[21] was used as the template to generate a PCR product using primers listed in Supplementary Table 1. The amplified PCR product was then cloned using the Gibson assembly reaction kit (New England Biolabs) into pLenti-CMV-Puro-Dest (w118-1) that was EcoRV digested. Vigilin cDNA (also known as HDLBP; MGC cDNA BC001179) was purchased from GE Dharmacon. The cDNA was amplified in two separate fragments using primers listed in Supplementary Table 1. Both PCR fragments were cloned by Gibson Assembly (New England Biolabs) into the EcoRV-digested third-generation lentiviral Gateway destination vector pLenti-CMV-Puro-Dest(w118-1), which drives transgene expression by a CMV promoter and harbours a puromycin-resistant gene as a selectable marker.

ER–GFP was engineered according to a previously reported construct[23]. Enhanced GFP (EGFP) fused with an N-terminal signal peptide of calreticulin and a C-terminal KDEL ER retention sequence was synthesized in two fragments (Integrated DNA Technologies) and cloned by Gibson Assembly (New England Biolabs) into the pLenti-CMV-Puro-Dest(w118-1) expression vector.

Lentiviral or retroviral transduction was used to create stable cell lines expressing a selected gene of interest. The respective genes of interest were cloned into the pLenti-CMV-Puro-DEST vector (w118-1; a gift from E. Campeau). Lentivirus was propagated by co-transfection of the transgene-expressing plasmid with a mixture of ΔVPR, VSV-G and pAdVAntage packaging plasmids into HEK293FT cells using FuGENE HD (Promega). The lentivirus was harvested from the supernatant and filtered through a 0.45-μm filter 48 h post-transfection. We then added 1×protamine sulphate to the lentivirus before transducing the respective cell lines overnight. Cells stably expressing the gene of interest were selected by treatment with 1–4 μg ml^{-1} puromycin over 2 d (InvivoGen) along with untransduced cells as negative controls. A lentivirus carrying either the *mCherry* (RFP) gene or the empty pLenti-CMV-Puro-DEST vector was used as a control for RRBP1 and vigilin complementation in the KO cell lines, respectively.

Quantitation of virus infectivity by qRT–PCR. Experiments where the vRNA loads were determined by quantitative PCR (qPCR) were performed as follows: 20,000 HEK293FT, Huh7.5.1 cells or their derivatives were seeded in triplicate in 96-well plates 1 d before infection. The cells were infected the next day with the indicated virus and m.o.i. The cells were lysed at the indicated times post-infection with the lysis buffer from the Ambion Power SYBR Green Cells-to-C_t kit (cat. no. 4402954). Reverse transcription and qPCR were performed according to the Cell-to-C_t kit instructions on a Bio-Rad CFX Connect qPCR machine. All C_t values were normalized to the expression values of 18S rRNA. The qRT–PCR primers are listed in Supplementary Table 1.

POWV infection, RNA extraction and qRT–PCR analysis. Cells were seeded in triplicate at 1×10^5 cells well^{-1} in a 24-well plate and incubated overnight. Following incubation, the DMEM medium was aspirated and the cells were washed twice with PBS. The cells were then infected with POWV (LB strain) at an m.o.i. of 0.1. At 48 h.p.i., the POWV-infected cells were washed twice with PBS and the cells were lysed in 350 μl RLT buffer (Qiagen). Total RNA was extracted using an

RNeasy mini kit (Qiagen). Complementary DNA was synthesized from 400 ng of total RNA template using the iScript cDNA synthesis kit (Bio-Rad). Primers targeting the positive-strand POWV genome (Supplementary Table 1) were used to quantify the POWV transcripts as a measure of POWV genome replication relative to the 18 s rRNA gene. To determine the efficient annealing temperature for the qPCR analysis, a gradient PCR was conducted using the Phusion high-fidelity PCR master mix with HF buffer (NEB), the cDNA template prepared from POWV-infected cell RNA, the two primer pairs and the following thermocycler conditions: 94 °C for 5 min; 32 cycles of 94 °C for 15 s, 62–68 °C for 30 s and 72 °C for 2 min; and 72 °C for 7 min. Following gel electrophoresis on E-gel 1.2% agarose with SYBR Safe (Life Technologies), an annealing temperature with amplicons of the expected size with no non-specific amplification was chosen. The qPCR reactions were performed on the Applied Biosystems QuantStudio 6 Flex real-time system (Life Technologies) in Micro-Amp optical 384-well reaction plates (Life Technologies). The QuantStudio real-time PCR software (v1.3) and the $\Delta\Delta C_t$ method were used to calculate the relative numbers of POWV transcripts.

Detection of DENV proteins using immunoblotting. Wild-type Huh7.5.1 cells and their derivatives were seeded in quadruplet at 1×10^5 cells well^{-1} in a 24-well plate and incubated overnight. The cells were then infected with DENV-2^{429557} at an m.o.i. of 0.1. The cells were harvested 72 h post-infection using RIPA buffer (TEKNOVA) supplemented with Laemmli sample buffer (Bio-Rad) and 5% β-mercaptoethanol (Bio-Rad). The cell lysates were then boiled for 10 min and separated by SDS–PAGE on pre-cast 4–15% polyacrylamide gels (Bio-Rad) in a Bio-Rad Mini-PROTEAN gel system. Proteins were transferred onto PVDF membranes. The PVDF membranes were blocked with PBS buffer containing 0.1% Tween 20 and 5% non-fat milk. The blocked membranes were then incubated overnight with primary antibody diluted in blocking buffer on a rocker at 4 °C. The primary antibodies were subsequently detected by incubating the membranes for 1 h at room temperature with secondary anti-mouse or anti-rabbit antibodies conjugated to horseradish peroxidase (Genetex; 1:5,000 dilution). The antibody-bound proteins were detected by incubating with SuperSignal West Pico PLUS chemiluminescent substrate or Dura Extended duration substrate (Thermo Fisher Scientific) peroxide solutions and visualized on a Bio-Rad ChemiDoc Touch imaging system. The following primary antibodies were used: anti-prM (Genetex, GTX128092) at a dilution of 1:2,500, anti-NS3 (Genetex, GTX124252) at a dilution of 1:2,500 and anti-GAPDH (Genetex, GTX 627408) at dilution of 1:5,000.

Luciferase reporter virus and DENV replicon luciferase assays. For the luciferase reporter virus assays, HEK293FT or Huh7.5.1 cells were seeded in 96-well plates (20,000 cells well^{-1} and 10,000 cells well^{-1}, respectively) and infected with DENV-Luc or ZIKV-Luc at an m.o.i. of 0.01. The final concentration of MK0608 was always 50 μM in this study. Cells were incubated with the viruses at 37 °C with 5% CO_2 and the cell lysates were harvested at the indicated times. Luciferase expression was measured using the *Renilla* luciferase assay system (Promega, E2820). The cells were lysed using *Renilla* lysis buffer, and luciferase activity was measured by the addition of the substrate and luciferase readings were immediately taken using Glomax 20/20 luminometer with a 5 s integration time.

For the *Renilla* luciferase-expressing DENV replicon assays, the DENV-replicon plasmid was linearized using XbaI restriction enzyme. Replicon RNA was generated using the MEGAscript T7 high yield transcription kit (Ambion, AM1334) with the reaction containing the 5 mM m^{7}G(5′)ppp(5′)G RNA cap structure analogue (NEB, S1405S). The resulting RNA was purified by sodium-acetate and ethanol precipitation. HEK293FT cells were washed twice with PBS and resuspended in electroporation buffer (Teknova, E0399). The purified replicon RNA (3 μg) was mixed with cells and the cells were electroporated using the Bio-Rad Gene Pulser Xcell electroporator with the square wave protocol. The electroporated cells were resuspended in cell culture medium without antibiotics and plated into 96-well plates. Luciferase expression was measured using the *Renilla* luciferase assay system (Promega E2820). The cells were lysed at the indicated times using *Renilla* lysis buffer, and the luciferase activity was measured by the addition of substrate and luciferase readings were taken immediately using Glomax 20/20 luminometer using a 5 s integration time.

irCLIP. Infrared crosslinking and immunoprecipitation was performed as previously reported[25]. A total of 7.5×10^6 Huh7.5.1 cells were seeded and infected the next day with DENV-2^{16681} or ZIKV^{PRVABC59} at an m.o.i. of 0.1. The infected cells were UV crosslinked at 48 h.p.i. to a total of 0.35 J cm^{-2}. Whole-cell lysates were generated in CLIP lysis buffer (50 mM HEPES, 200 mM NaCl, 1 mM EDTA, 10% glycerol, 0.1% NP-40, 0.2% Triton X-100 and 0.5% *N*-lauroylsarcosine) and briefly sonicated using a probe-tip Branson sonicator to solubilize the chromatin. Each experiment was normalized to the total protein amount, typically 1 mg, and partially digested with RNase A (Thermo Fisher Scientific, EN0531) for 10 min at 37 °C and then quenched on ice. The RRBP1 (Bethyl, A303-996A), vigilin (Bethyl, A303-971A) and IgG (Thermo Fisher Scientific, 02-6102) immunoprecipitations were performed using 15 μg of each antibody with 50 μl Protein A Dynabeads (Thermo Fisher Scientific) for 8 h at 4 °C with rotation. The samples were sequentially washed (1 min each wash) at 25 °C in 1-ml volumes as follows: 1×high stringency buffer (15 mM Tris–HCl, pH 7.5, 5 mM EDTA, 2.5 mM EGTA, 1% Triton X-100, 1% sodium deoxycholate, 120 mM NaCl and 25 mM KCl), 1×high salt buffer (15 mM Tris–HCl, pH 7.5, 5 mM EDTA, 2.5 mM EGTA, 1% Triton X-100, 1% sodium deoxycholate and 1 M NaCl) and 2×NT2 buffer (50 mM Tris–HCl, pH 7.5, 150 mM NaCl, 1 mM $MgCl_2$ and 0.05% NP-40). The RNA–protein complexes were dephosphorylated after the NT2 washes with T4 PNK (NEB) for 45 min in an Eppendorf Thermomixer at 37 °C, 15 s at 1,400 r.p.m., 90 s of rest in a 30 μl reaction, pH 6.5, containing 10 U T4 PNK, 0.1 μl SUPERase-IN (Thermo Fisher Scientific) and 6 μl PEG 400 (16.7% final). The dephosphorylated RNA–protein complexes were then rinsed once with NT2 buffer and 3′-end ligated overnight with T4 RNA ligase 1 (NEB) in an Eppendorf Thermomixer at 16 °C, 15 s at 1,400 r.p.m., 90 s of rest in a 60 μl reaction containing 10 U T4 RNA ligase, 1.5 pmol pre-adenylated-IR800-3′ biotin DNA-adaptor, 0.1 μl SUPERase-IN and 6 μl of PEG 400 (16.7% final). The following day, the samples were rinsed once with 500 μl NT2 buffer and resuspended in 30 μl of 20 mM dithiothreitol (DTT) and 1×LDS (Thermo Fisher Scientific) in NT2 buffer. The samples were heated to 75 °C for 10 min and the released RNA–protein complexes were separated by 4–12% bis-Tris SDS–PAGE (1.0 mm × 12 well) at 200 V for 45 min. The resolved ribonucleoprotein complexes were wet-transferred to nitrocellulose at 550 mA for 45 min at 4 °C.

The nitrocellulose membranes were imaged using an Odyssey CLx scanner (LiCor); the RBP–RNA complexes were excised using scalpels and the RNA was recovered by adding 0.1 ml Proteinase K reaction buffer (100 mM Tris, pH 7.5, 50 mM NaCl, 1 mM EDTA and 0.2% SDS) and 5 μl 20 mg ml^{-1} Proteinase K (Thermo Fisher Scientific). The proteins were digested for 60 min at 50 °C in an Eppendorf Thermomixer. Next, 200 μl saturated-phenol–chloroform pH 6.7 was added to each tube and incubated for 10 min at 37 °C in an Eppendorf Thermomixer with 1,400 r.p.m. The tubes were briefly centrifuged and the entire contents transferred to a 2 ml Heavy Phase Lock Gel (5Prime, cat. no. 2302830). The samples were centrifuged for 2 min at >13,000 r.p.m. The aqueous layer was re-extracted with 1 ml chloroform (inverting ten times to mix; no vortexing) in the same 2 ml Phase Lock Gel tube and centrifuged for 2 min at >13,000 r.p.m. The aqueous layer was then transferred to a new 2 ml Heavy Phase Lock Gel tube and extracted again with an additional 1 ml chloroform. After a 2 min centrifugation at >13,000 r.p.m., the aqueous layer was transferred to a siliconized 1.5 ml tube and precipitated overnight at −20 °C with the addition of 10 μl 5 M NaCl, 3 μl linear polyacrylamide (Thermo Fisher Scientific) and 0.8 ml 100% ethanol. The RNA fragments were pelleted at >13,000 r.p.m. for 45 min at 4 °C, washed once with 1 ml ice-cold 75% ethanol and air dried.

The RNA pellets were resuspended in 12 μl water; 1 μl of 3 μM cDNA and 1 μl of 10 mM dNTPs were added, heated to 70 °C for 5 min and then rapidly cooled to 4 °C. We then added cDNA master mix (4 μl 5×SuperScript IV (SSIV) buffer, 1 μl 100 mM DTT and 1 μl SuperScript IV; 6 μl total) to the annealed RNA and incubated for 30 min at 55 °C. The cDNA:RNA hybrids were captured by the addition of 5 μl MyOne Streptavidin C1 Dynabeads (Thermo Fisher Scientific), which had been rinsed and suspended in 50 μl Biotin IP buffer (100 mM Tris, pH 7.5, 1 M NaCl, 1 mM EDTA and 0.1% Tween), and end-over-end rotation for 45 min at room temperature. The beads were placed on a 96-well magnet and washed twice sequentially with 100 μl Biotin IP buffer and 100 μl ice-cold 1 × PBS. The beads were resuspended in 10 μl cDNA elution buffer (8.25 μl water, 1 μl of 1 μM P3 short oligo and 0.75 μl of 50 mM $MnCl_2$) and heated to 95 °C for 10 min. Subsequently, samples were cooled down at a rate of 0.1 °C s^{-1} to 60 °C. Next, 5 μl circularization reaction buffer (3.3 μl water, 1.5 μl 10×Circligase II buffer and 0.5 μl Circligase II; Epicentre) was added. The cDNA was circularized for 2 h at 60 °C, followed by purification with 30 μl AMPure XP beads (Beckman Coulter) and 75 μl isopropanol. The samples were incubated for 20 min at 25 °C, washed twice with 100 μl 80% ethanol, air dried for 5 min and eluted in 14 μl water. Elution took place at 95 °C for 3 min and the samples were immediately transferred to a 96-well magnet. The eluted cDNA was transferred to a new PCR tube containing 15 μl 2×Phusion HF-PCR master mix (NEB), 0.5 μl of 30 μM P3/P6 PCR oligo mix and 0.5 μl 15×SYBR Green I (Thermo Fisher Scientific). Real-time qPCR was then performed as follows: 98 °C for 2 min; 15 cycles of 98 °C for 15 s, 65 °C for 30 s and 72 °C for 30 s, with data acquisition set to the 72 °C extension step. The PCR reactions were cleaned by adding 4.5 μl isopropanol, 54 μl AMPure XP beads and incubating for 10 min. The beads were washed once with 80% ethanol, dried for 5 min and eluted in 15 μl water. Illumina flow cell adaptors were added by adding 15 μl 2×Phusion HF-PCR master mix and 0.4 μl P3solexa/P6solexa oligo mix and amplified as follows: 98 °C for 2 min, followed by three cycles of 98 °C for 15 s, 65 °C for 30 s and 72 °C for 30 s. The final libraries were purified with the addition of 48 μl AMPure XP beads and incubation for 5 min. The beads were washed twice with 70% ethanol, dried for 5 min and eluted in 20 μl water. The libraries (1–2 μl) were quantitated using a HS-DNA Bioanalyzer. The samples were deep sequenced on the Illumina NextSeq machine (single-end, no index, high-output, 75-base-pair cycle run).

Analysis of irCLIP data. The irCLIP data were processed using the FAST-iCLIP pipeline (https://github.com/ChangLab/FAST-iCLIP/tree/lite). PCR duplicates were removed using unique molecular identifiers in the RT primer region. The adaptor and barcode sequences were trimmed and reads were mapped step-wise to viral (DENV or ZIKV), repetitive and finally non-repetitive (GRCh38) genomes. Bowtie2 indexes were generated using the 'bowtie2-build' command in Bowtie2

for the DENV (KU725663.1) and ZIKV (KU501215.1) RNA genome sequences. The specific parameters used for the FAST-iCLIP pipeline were as follows: -f 18 (trims 17 nt from the 5′ end of the read), -l 16 (includes all reads longer than 16 nt), –bm 29 (minimum MAPQ score from bowtie2 of 29 is required for mapping; unique mapping only), –tr 2,3 (repetitive genome) and –tn 2,3 (non-repetitive genome) RT stop intersection (n,m; where n = replicate number and m = number of unique RT stops required per n replicates). Using the –tr/tn 2,3 parameters, a minimum of six RT stops are required to support any single nucleotide identified as a crosslinking site. For the Gene Ontology analysis, the top 25% of the irCLIP-bound genes were analysed using the Database for Annotation, Visualization and Integrated Discovery (DAVID) tool (https://david.ncifcrf.gov/tools.jsp). The peaks of the RT stops were called on the biologically replicated intersection of the RT stop positions using iCount peaks (http://icount.readthedocs.io/en/latest/). The command line was as follows: iCount peaks gencode.v21.annotation.segment.gtf RTstop_input.bed Out_iCpeaks.bed —scores Out_iCpeaksScores.tsv. Regions from 'Out_iCpeaks.bed' were then annotated with HOMER (http://homer.ucsd.edu/homer/) using the following command: annotatePeaks.pl Out_iCpeaks.bed hg38 > Out_iCpeaks_hg38_HOMERanno.txt -annStats Out_iCpeaks_hg38_HOMERanno_stats.txt.

CLIP mass spectrometry. Cells were grown and UV crosslinked, and lysates were generated, RNase A treated, immunoprecipitated and washed as described for irCLIP. No dephosphorylation or RNA ligation took place, but the RBP–RNA complexes were denatured and run in SDS–PAGE gels as per the irCLIP procedure. After a complete run of the SDS–PAGE, the gels were fixed and stained with a Colloidal blue staining kit (Thermo Fisher Scientific) as per the manufacturer's instructions. The stained gels were visualized with the Odyssey CLx scanner and regions of each lane were excised based on where the predicted RBP–RNA complex would migrate.

The gel slices were prepared for mass spectrometry by sequentially rinsing in 200 µl HPLC-grade water, 100% acetonitrile (ACN; Thermo Fisher Scientific) and 50 mM ammonium bicarbonate (AmBic). The samples were reduced by adding 200 µl of 5 mM DTT in 50 mM AmBic and incubating at 65 °C for 35 min. The reduction buffer was discarded and the samples were cooled to room temperature. Alkylation was achieved by adding 200 µl of 25 mM iodoacetamide in 50 mM AmBic for 20 min at 25 °C in the dark. The alkylation buffer was discarded; the samples were rinsed once in 200 µl of 50 mM AmBic and then washed twice for 10 min each in 200 µl freshly prepared 50% ACN in 50 mM AmBic. After each wash, the supernatant was discarded and the samples were dried for 3 h using a SpeedVac. Once dry, the proteins were digested by adding 100 ng trypsin in 200 µl of 50 mM AmBic for 16 h at 37 °C. The samples were subsequently acidified by adding formic acid to a final concentration of 2.5% and incubating at 37 °C for 45 min. Finally, the samples were desalted using HyperSep filter plates with a 5–7 µl bed volume (Thermo Fisher Scientific) following the manufacturer's instructions. The samples were eluted three times in 100 µl 80% ACN in 2.5% formic acid, dried on a SpeedVac and resuspended in 10 µl 0.1% formic acid for mass-spectrometry analysis. Desalted peptides were analysed by online capillary nanoLC–MS/MS. The samples were separated using a 20-cm reversed phase column fabricated in-house (inner diameter of 100 µm, packed with ReproSil-Pur C18-AQ 3.0 µm resin (Dr. Maisch GmbH)), which was equipped with a laser-pulled nano-electrospray emitter tip. Peptides were eluted at a flow rate of 400 nl min^{-1} using a two-step linear gradient of 2–25% buffer B in 70 min and 25–40% B in 20 min (buffer A: 0.2% formic acid and 5% DMSO in water; buffer B: 0.2% formic acid and 5% DMSO in ACN) in an Eksigent ekspert nanoLC-425 system (AB Sciex). The peptides were ionized with electrospray ionization into an Orbitrap Elite Hybrid Ion Trap-Orbitrap mass spectrometer (Thermo Fisher Scientific). The instrument method parameters were as follows: MS1 resolution, 60,000 at 400 m/z; scan range, 340−1,600 m/z. The top-20 most-abundant ions were subjected to collision-induced dissociation with a normalized collision energy of 35%, activation q of 0.25 and precursor isolation width of 2 m/z. Dynamic exclusion was enabled with a repeat count of one, a repeat duration of 30 s and an exclusion duration of 20 s. FASTA sequences of the DENV (accession number: ANG57776) or ZIKV (accession number: AOR51315) proteomes were downloaded and appended to the human proteome (UniProt accession number: UP000005640) for each database search. RAW files were searched using Byonic (Protein Metrics) with the following parameters: semi-specific cleavage specificity at the C-terminal site of R and K, allowing for two missed cleavages, precursor mass tolerance of 12 ppm and fragment ion mass tolerance of 0.4 ppm. Methionine oxidation, asparagine deamidation and N-term acetylation were set as variable modifications. Cysteine carbamidomethylation was set as a fixed modification. Peptide hits were filtered using a 1% FDR.

A custom Python script was written to merge technical and biological replicates across the different ChIRP-MS experiments (https://github.com/jasonkli/MS-Analysis). First, .xls output files from Byonic were analysed for spectra of each protein identified. The total number of spectra, excluding any spectra with a quality score below 100, were counted and printed into new .xls files, one for each set of experiments. For each set of technical replicates, the number of spectra for each protein is summed across replicates and normalized by dividing by the total number of spectra from all reads in the set. These normalized values were then scaled with a factor of 1,000 for readability. Next, we consolidated data across biological replicates. We filtered identified proteins so that a given protein was required to be present with at least one spectrum in each biological replicate. The normalized spectra of the surviving protein IDs were then averaged across the biological replicates. Finally, a combined table was generated across all experimental data as per the previous steps. For each protein identified, we output the following information: common gene name, UniProt ID, comma-separated values of the raw spectra from each technical and biological replicate, the average normalized spectra from each experiment (with an added correction factor of one to avoid any zeroes for subsequent analyses), the averaged normalized spectra divided by the number of amino acids in the protein and the total amino acids in that protein.

Comprehensive identification of RNA-binding proteins by mass spectrometry. DENV-, ZIKV- and RV-targeting probes were designed using online tools available at https://www.biosearchtech.com/stellaris, with a repeat masking setting of three and even coverage of the whole transcript. The full probe sequences are available in Supplementary Table 1. Oligos were synthesized with 3′ biotin-TEG modification at the Stanford Protein and Nucleic Acid Facility.

ChIRP-MS was performed largely as described in Chu and colleagues[9]. Huh7.5.1 cells ($9 \times 7.5 \times 10^6$) were seeded and infected the following day with DENV-2 (16681 strain-Hap1 adapted), ZIKV PRVABC59 at an m.o.i. of 0.1 or mock-treated in triplicate ($3 \times 3 = 9$ flasks per condition). For RV, $2 \times 7.5 \times 10^6$ H1-HeLa cells were seeded and infected the next day at an m.o.i. of 1 or mock infected. The medium was aspirated 48 h after infection, and the cells were rinsed once with 10 ml PBS per flask, trypsinized, pelleted at 1,400 r.p.m. for 5 min and washed twice with PBS. The cells were then resuspended in 3% formaldehyde containing PBS and rocked for 30 min at 25 °C. Chemical crosslinking was then stopped by the addition of glycine to a final concentration of 125 mM for 5 min at 25 °C. The crosslinked cells were pelleted at 2,000 r.p.m. for 5 min (the supernatant was discarded) and flash frozen at −80 °C for storage. Lysate was generated by resuspending the cell pellets in 1 ml lysis buffer (50 mM Tris–HCl, pH 7.0, 10 mM EDTA and 1% SDS) per 100 mg cell pellet (pellet volume of about 100 µl). The lysates were sonicated using a focused-ultrasonicator (Covaris, E220) until the average RNA length was 500 nucleotides, as determined by agarose gel analysis, and stored at −80 °C. Stored lysates were thawed on ice; 2 ml of freshly prepared ChIRP hybridization buffer (750 mM NaCl, 1% SDS, 50 mM Tris–HCl, pH 7.0, 1 mM EDTA and 15% formamide) was added for every millilitre of sonicated lysate and the lysates were pre-cleared by adding 30 µl washed MyOne C1 beads per 1 ml lysate at 37 °C for 30 min on rotation. Beads were removed twice from the lysate using a magnetic stand; for this and all subsequent magnetic stand steps we allowed >1 min of separation before removing any supernatant. Next, 1.5 µl of 100 µM ChIRP Probe Pools was added per millilitre of lysate. ChIRP Probe Pools (Supplementary Table 1) for control, DENV or ZIKV enrichments were made by mixing equal volumes of 99 (DENV + ZIKV), 50 (DENV) or 49 (ZIKV) individual antisense oligos at 100 µM (final concentration of 1.01, 2 and 2.04 µM for each probe, respectively). The RV pool was made by mixing equal volumes of 50 individual antisense oligos targeting the RV genome at 100 µM (2 µM final concentration for each probe) and was used for the RV-uninfected control. After mixing, hybridization took place on rotation for 16 h at 37 °C. Subsequently, 150 µl washed MyOne C1 beads per millilitre of lysate were added to each sample and incubated on rotation for 45 min at 37 °C. The enriched material was collected on the beads with a magnetic stand and the beads were washed 5 × 2 min in 1 ml ChIRP wash buffer (2×SSC solution (Thermo Fisher Scientific) and 0.5% SDS) at 37 °C. To elute the enriched proteins, the beads were collected on a magnetic stand, resuspended in ChIRP biotin elution buffer (12.5 mM biotin, 7.5 mM HEPES, pH 7.9, 75 mM NaCl, 1.5 mM EDTA, 0.15% SDS, 0.075% sarkosyl and 0.02% sodium deoxycholate), mixed at 25 °C for 20 min on rotation and at 65 °C for 15 min with shaking. The eluent was transferred to a fresh tube and the beads were eluted again. The two eluents were pooled (about 1,200 µl) and residual beads were removed again using the magnetic stand. Trichloroacetic acid (25% of the total volume; 300 µl) was added to the clean eluent, vortexed and the samples were then placed overnight at 4 °C for precipitation. The next day, the proteins were pelleted at 21,000 g at 4 °C for 45 min. The supernatant was carefully removed and the protein pellets were washed once with ice-cold acetone. The samples were spun at 21,000 r.c.f. for 5 min at 4 °C. The acetone supernatant was removed, the tubes were briefly centrifuged again and—after the removal of the residual acetone—were left to air-dry on the bench top. The proteins were then solubilized in 1×LDS buffer in NT2 with 20 mM DTT and boiled at 95 °C for 30 min with occasional mixing for reverse-crosslinking.

The protein samples were size-separated on bis-Tris SDS–PAGE gels (Bio-Rad), fixed and stained with colloidal blue, and prepared for mass-spectrometry analysis as described for 'CLIP mass spectrometry'. Biological triplicates were performed for each uninfected control, DENV or ZIKV ChIRP-MS. Each replicate was cut into four slices in the SDS–PAGE and prepared independently (total of four mass spectrometry runs per biological replicate). For RV ChIRP-MS, one replicate of RV-infected and uninfected H1-HeLa cells was used and split across four independent gel slices. ChIRP-MS data were searched with Byonic and processed as per the custom python script described in 'CLIP mass spectrometry'. Principal

component analysis of the individual biological replicates was accomplished using the ClusterVis tool (http://biit.cs.ut.ee/clustvis/)[49]. High-confidence host factors associated with vRNAs were defined as being enriched more than twofold over the uninfected cell ChIRP. We used the SAINT scoring system[50], specifically the SAINTq software (http://saint-apms.sourceforge.net/Main.html), to apply a statistical confidence filter to refine the ChIRP-MS hits. Individual biological triplicates for mock-, DENV- or ZIKV-infected ChIRP-MS hits were used as input data for the SAINTq software with default settings for the FDR calculations.

ChIRP qRT–PCR. Cells were grown, infected, crosslinked and sonicated as described earlier. After sonication, 1% of the lysate was removed and saved as an 'input' sample. The lysates were again processed as earlier for pre-clearing, hybridization, MyOne C1 capture and bead washing. After washing, 1% of each sample was removed as an 'enriched' fraction. The enriched fractions were collected while the MyOne C1 beads were fully resuspended in ChIRP wash buffer. ChIRP PK buffer (10 mM Tris–HCl pH 7.0, 100 mM NaCl, 1 mM EDTA, 0.2% SDS) was added to the input and enriched samples to a final volume of 95 µl. Proteinase K (5 µl of 20 mg ml^{-1}) was then added with shaking at 55 °C for 45 min to digest the protein. RNA was extracted by adding 500 µl TRIzol (Thermo Fisher Scientific), incubating at 55 °C for 5 min and then adding 100 µl chloroform. After mixing each sample by vortexing for 7 s, the samples were incubated at 25 °C for 5 min and then centrifuged at 12,000 r.p.m. for 15 min at 4 °C. The aqueous layer was carefully removed from each sample, mixed with two volumes of 100% ethanol and purified using a RNA Clean & Concentrator-25 kit (Zymo Research) as per the manufacturer's instructions. All RNA samples were DNase treated with the Turbo DNA-free kit (Thermo Fisher Scientific). SuperScript VILO (Thermo Fisher Scientific) was used to generate cDNA according to manufacturer's instructions. The qPCR analyses were performed on the CFX96 Touch real-time PCR detection system (Bio-Rad). All of the primers used are provided in Supplementary Table 1.

ChIRP and RNA Bioanalyzer. Cells were grown, infected and the RNA was harvested as described earlier. This RNA was either analysed directly using a RNA Pico Bioanalyzer chip (Agilent Technologies) or by denaturing gel electrophoresis. A formaldehyde-agarose gel was made using the NorthernMax kit (Thermo Fisher Scientific) as per the manufacturer's protocol. The RNA samples were denatured in 0.5×Gel Loading Buffer II (Thermo Fisher Scientific) and 1×SybrGold (Thermo Fisher Scientific) at 55 °C for 10 min, cooled on ice for 3 min and then loaded into the gel. After running at 110 V for 35 min, the RNA was imaged using a UV transilluminator.

RNA-seq from irCLIP samples. Input material for RNA-seq was obtained from the same lysates generated for the irCLIP experiment. After lysis and sonication, as described earlier, 100 µl lysate from each biological duplicate of the uninfected and DENV- or ZIKV-infected cells was removed. Proteins were digested and RNA extracted with Proteinase K and TRIzol as described in the 'ChIRP qRT–PCR' section. Ribosomal RNA was depleted using a RiboMinus transcriptome isolation kit (human/mouse; Thermo Fisher Scientific) as per the manufacturer's instructions starting with 5 µg total RNA per sample. Samples depleted of rRNA were fragmented using the RNA fragmentation reagent (Thermo Fisher Scientific) at 90 °C for 30 s. After fragmentation, the RNA samples were purified using a RNA Clean & Concentrator-5 kit (Zymo Research) as described in the 'ChIRP qRT–PCR' section and the RNA was eluted in 5 µl water. The RNA 3′ ends were repaired by the addition of 0.5 µl 10×T4 PNK buffer (New England Biolabs), 1 µl T4 PNK, 1 µl FastAP (Thermo Fisher Scientific), 1 µl RiboLock (Thermo Fisher Scientific) and 1.5 µl water for 45 min at 37 °C. Next, a 3′-adaptor was ligated to the RNA samples by directly adding 1 µl 10×T4-RNL1 buffer (New England Biolabs), 1 µl T4-RLN1 (New England Biolabs), 1 µl of 100 mM DTT, 0.75 µl of 3 µM irCLIP 3′-adaptor and 6 µl 50% PEG8000 (New England Biolabs) for 4 h at 25 °C. After the completion of the ligation reaction, unligated 3′-adaptors were digested by directly adding 2.5 µl Rec-Jf (New England Biolabs), 1.25 µl 5′-deadenylase (Epicentre), 3 µl 10×5′-deadenylase buffer (Epicentre) and incubating for 1 h at 37 °C. The samples were purified using a RNA Clean & Concentrator-5 kit (Zymo Research) as above. The ligated and purified RNA samples were processed further into double-stranded DNA libraries as per the final steps of the irCLIP procedure described earlier. The samples were sequenced on the NextSeq 500 platform (Illumina) after library quantification and pooling. Data were processed for mapping as per the irCLIP pipeline; however, RT stops were not isolated after mapping. Instead the featureCount tool of the Subread package (version 1.6.0) was used to count the aligned reads supporting transcripts annotated from Gencode Release 26 (GRCh38; https://www.gencodegenes.org/releases/26.html). Genes supported by at least ten reads in a biological replicate were considered as expressed. RNA-seq counts were normalized to the total counts for all expressed genes in each sample to produce counts-per-million reads. To calculate the enrichment of ER-annotated genes, a counts-per-million cut-off of 1.0 was set for genes identified in the uninfected RNA-seq (18,199) and then intersected with ER-annotated gene names from Uniprot (Supplementary Table 4). A two-sided Fisher's exact test was used to determine statistical enrichment.

Immunofluorescence and RNA fluorescence in situ hybridization. Huh7.5.1 cells (80,000) were seeded on poly-lysine-coated glass cover slips in a 24-well format. The cells were infected the following day with either DENV-2 or ZIKV (Puerto Rico) at an m.o.i. of 1 for 24 h. The cells were fixed with 4% formaldehyde (Sigma), washed with PBS and permeabilized using the Immunofluorescence application solution kit according to the manufacturer's recommendations (Cell Signaling, cat. no. 12727). The ER–GFP marker was transfected into Huh7.5.1 cells using Lipofectamine 3000 (Thermo Fisher Scientific) according to the manufacturer's guidelines. At 48 h post-transfection, the cells were fixed with 4% formaldehyde for 30 min at room temperature, washed with PBS and permeabilized with 1% NP-40 for 5 min at room temperature. The cells were incubated with antibodies against RRBP1 (Bethyl, A303-996A; 1:100 dilution), vigilin (Bethyl, A303-971A; 1:20 dilution), GFP (Thermo Fisher Scientific, MA5-15256; 1:100 dilution) for 90 min at room temperature. The cells were washed twice with PBS and stained with secondary Alexa Fluor antibodies 488 nm, 594 nm, 647 nm (Thermo Fisher Scientific, cat. nos A-11034, R37117 and A31573) at a 1:200 dilution for 1 h at room temperature. RNA probes that detect the positive-strand vRNA for DENV and ZIKV were purchased from Affymetrix. The vRNAs were then stained using RNA probes in conjunction with branched-DNA amplification to generate single molecule detection of vRNA as per the manufacturer's protocol (ViewRNA Cell Plus Assay, cat. no. 88-19000-99). Finally, coverslips were mounted onto glass slides using PermaFluor (Thermo Fisher Scientific) containing 4′,6-diamidino-2-phenylindole (DAPI; Affymetrix). The cells were visualized on a Nikon AR1 or Leica SP8 confocal microscope. At least 30 cells were analysed for each condition using the ImageJ colocalization algorithm COLOC2 (https://github.com/fiji/Colocalisation_Analysis/releases/tag/Colocalisation_Analysis-3.0.0). Pearson's correlation scores for colocalization were plotted to determine the level of colocalization between the vRNAs and either the costained host proteins or DAPI.

Subcellular fractionation. Huh7.5.1 cells (300,000) were washed twice with cold PBS. The cells were then separated into their cytosolic and ER compartments as previously described[24]. Briefly, the cytosol fraction was extracted by the addition of a buffer containing 0.03% digitonin, 110 mM potassium acetate, 25 mM K-HEPES pH 7.2, 15 mM $MgCl_2$ and 4 mM $CaCl_2$ to the dish and incubated on ice for 5 min. The supernatant with the buffer containing the cytosolic contents was collected after low-speed centrifugation (600 r.c.f. for 5 min) and the cells were washed with the same buffer containing 0.0015% digitonin. The first lysis and the wash were combined and represent the cytosolic contents of the cell. The membrane fraction that contained the ER membranes was then collected by lysis of the digitonin-extracted cell pellet with an ER lysis buffer containing 2% *n*-dodecyl-β-D-maltoside, 200 mM potassium acetate, 25 mM K-HEPES pH 7.2, 15 mM $MgCl_2$ and 4 mM $CaCl_2$. Western blot analysis of the two different fractions was then performed with antibodies against RRBP1, vigilin, the cytoplasmic markers GAPDH (Genetex, GTX 627408) and tubulin (Abcam ab97872), and the ER marker RPN1 (Bethyl Laboratories, A305-026A).

Native co-IP. Huh7.5.1 cells were seeded in six-well plates and infected with DENV-2 at an m.o.i. of 0.1 or with no virus as described earlier. Protein-G beads were pre-conjugated to rabbit-IgG (Thermo Fisher Scientific, 02-6102) or anti-RRBP1 (Bethyl, A303-996A) antibodies; 3 µg antibody and 10 µl Protein G beads were used per immunoprecipitation reaction. After 48 h of infection, protein lysate was generated by adding 650 µl co-IP lysis buffer (10 mM HEPES, 2 mM $MgCl_2$, 10 mM KCl, 0.5% NP-40, 0.5 mM EDTA and 150 mM NaCl) to each well, disrupting the cells with a cell lifter and incubating the lysate at 4 °C for 30 min. The lysates were cleared by centrifugation at 5,200 r.c.f for 5 min at 4 °C. The clarified lysates (100 µl) from the no-virus or DENV-2 infections were diluted in 400 µl co-IP lysis buffer (500 µl final), to which the pre-conjugated antibody–Protein-G beads were added for 3 h at 4 °C with rotation. Each condition was performed in biological triplicates. RNase-treated samples were generated by adding 1 µl of 1 µg µl^{-1} RNase A to the lysate during the immunoprecipitation at 4 °C. After 3 h, each sample was washed three times with 750 µl co-IP lysis buffer and once with 750 µl NT2 buffer. The enriched proteins were subsequently analysed by western blotting.

Genome-scale CRISPR–Cas9 KO screens. Genome-scale CRISPR–Cas9 mutagenized Huh7.5.1 cells were generated as previously described[16,51]. In brief, stable Cas9-expressing Huh7.5.1 WT cells were engineered by transducing lentiCas9-Blast and selected using blasticidin. Subsequently, 300×10^6 Cas9-expressing Huh7.5.1 cells were transduced with the lentiGuide-Puro from the GeCKOv2 library[51] at an m.o.i. of 0.3. Puromycin-resistant cells were selected, pooled and expanded. These mutagenized cells were ready to be used for CRISPR genetic screens at 10 d post-transduction. Mutagenized cells—65×10^6 per library (A and B)—were seeded for 16 h and then subjected to the following DENV infections: DENV-1^{276RKI} (m.o.i. = 0.4 plaque-forming units (p.f.u.) cell^{-1}), DENV-2^{429557} (m.o.i. = 0.05 p.f.u. cell^{-1}), DENV-3$^{Philippines/H871856}$ (m.o.i. = 0.003 p.f.u. cell^{-1}) and DENV-4$^{BC287/97}$ (m.o.i. = 0.1 p.f.u. cell^{-1}). Cytopathic effects were observed as early as 4 d post-infection. Populations of virus-resistant cells were harvested 19–24 d post-infection. Uninfected starting populations of mutagenized cells were used as the unselected reference. Total genomic DNA from both virus-resistant and uninfected cells was extracted using a QIAamp DNA mini kit (Qiagen). The inserted guide RNA sequences were retrieved from the genomic DNA by PCR amplification using the primers F1 and R1 (Supplementary Table 1). The PCR products were further

barcoded by an additional round of PCR amplification using the specific primers listed in Supplementary Table 1. The barcoded PCR products were then purified and subjected to next-generation sequencing on a NextSeq platform (Illumina) using a custom next-generation sequencing primer (Supplementary Table 1). The sequencing data were processed and analysed using the MAGeCK algorithm to determine the ranking of each hit by taking the following criteria into account: the number of sequencing reads per unique guide, the number of unique guide RNA per gene (that is, 0–6) and the enrichment of a particular guide RNA in comparison to uninfected cell populations[52]. The separate next-generation sequencing FASTQ files for all four DENV serotypes were concatenated into one file and subsequently subjected to MAGeCK analysis. For the Gene Ontology analysis, the top-50 hits of pan-DENV serotypes CRISPR KO screens were analysed using DAVID[53] (https://david.ncifcrf.gov/tools.jsp).

Haploid genetic screens. The haploid genetic screens were performed as previously described[45,54]. Briefly, $3\times100\times10^6$ gene-trap mutagenized HAP1 cells were seeded and infected with the following ZIKV strains (m.o.i. of 1): $ZIKV^{FLR}$ (Colombia strain), $ZIKV^{PRVABC59}$ and $ZIKV^{H/PF/2013}$. The medium was aspirated 48 h post-infection and replaced with fresh IMDM medium containing 10% FBS. Clear cytopathic effects were observed at 2 and 3 d after infection, leading to death of the majority of cells. Resistant HAP1 colonies were harvested 10 d after infection (yield of approximately 30×10^6 cells per virus strain) and the genomic DNA was isolated. Gene-trap insertion sites were determined by linear amplification of the genomic-DNA flanking regions of the gene-trap DNA insertion sites using linear-amplification-mediated PCR. Briefly, genomic DNA from selected and unselected populations (approximately 40×10^6 cells per condition) were isolated using a QIAamp mini kit (Qiagen). The isolated genomic DNA was then separately digested using the restriction enzymes MseI and SpeI, and the resulting digested DNA products from both digestion reactions were pooled for each condition. A linear PCR using biotinylated primers recognizing the long terminal repeat (Supplementary Table 1) of the gene-trap was performed using the AccuPrime PCR kit from Invitrogen. A DNA-linker primer (Supplementary Table 1) was then ligated to the linear-amplification mediated PCR products on beads using the Circligase II kit (Epicentre). Biotinylated PCR products were then isolated using magnetic streptavidin beads provided with the Dynal kilobaseBINDER kit (Invitrogen). A final PCR using primer sets with Solexa adaptor sequences (Supplementary Table 1) and bar codes was then used to amplify the isolated fragments with different sizes. The final PCR products were checked on a 2% agarose gel and sent for sequencing on an Illumina NextSeq platform. The reads were aligned to the human genome using Bowtie and enrichment of independent insertions was calculated as previously described[16]. The *P* value (corrected for FDR) for each gene identified in the screen was determined using a one-sided Fisher's exact test run in the R software environment. If the *P* value was lower than the R software could report, the corrected *P* value was set to the smallest non-zero normalized floating-point number R could report, that is, $\sim1\times10^{-307}$(ref. [54]). The screens were individually compared with the unselected dataset or the fastq files were first merged to detect genes common to the three screens. For the Gene Ontology analysis, the top-50 hits of the ZIKV haploid genetic screens were analysed using DAVID (https://david.ncifcrf.gov/tools.jsp).

RNA stability and northern blot analysis. The 3′ UTR of the DENV-2^{16681} infectious clone (nucleotides 10,205–10,704) was PCR amplified (Supplementary Table 1) and Zero-Blunt cloned into the pCR-Blunt plasmid (Thermo Fisher Scientific). This plasmid served as a template to generate northern blot probes that hybridized to the 3′ UTR of DENV-2. To prepare cell lysates for northern blotting, 2×10^6 cells (WT or RRBP1-vigilin double KO) on a 60-mm dish were first infected with DENV-2^{16681} for 48 h at an m.o.i. of 0.25 p.f.u. $cell^{-1}$. MK0608 (50 μM final concentration) was introduced to the infected cells at 48 h.p.i. to block further replication of DENV-2. The cells were washed twice with cold PBS and harvested in TRIzol (Thermo Fisher Scientific) at designated time points post-MK0608 treatment. Total RNA was extracted using the RNeasy mini kit (Qiagen) following the manufacturer's protocol. For the northern blot analysis of DENV vRNA, 10 μg total RNA in RNA loading buffer (32% formamide, 1×MOPS–EDTA–sodium acetate (MESA, Sigma) and 4.4% formaldehyde) were denatured for 20 min at 70 °C, separated in a 1.2% agarose gel containing 1×MESA and 3.7% formaldehyde, transferred overnight and UV crosslinked to a Zeta-probe membrane (Bio-Rad). The membrane was blocked and hybridized using ExpressHyb hybridization buffer (Clontech) and α-^{32}P dATP-RadPrime-labelled DNA probes. Densitometry analysis of the bands was performed using the ImageJ open access software.

Reporting Summary. Further information on research design is available in the Nature Research Reporting Summary linked to this article.

Data availability

The raw and processed sequencing data can be found at https://www.ncbi.nlm.nih.gov/geo/query/acc.cgi?acc=GSE109194.

Received: 21 November 2018; Accepted: 23 April 2019;
Published online: 05 August 2019

References

1. Bhatt, S. et al. The global distribution and burden of dengue. *Nature* **496**, 504–507 (2013).
2. Shepard, D. S., Undurraga, E. A., Halasa, Y. A. & Stanaway, J. D. The global economic burden of dengue: a systematic analysis. *Lancet Infect. Dis.* **16**, 935–941 (2016).
3. Kaufmann, S. H. E., Dorhoi, A., Hotchkiss, R. S. & Bartenschlager, R. Host-directed therapies for bacterial and viral infections. *Nat. Rev. Drug Discov.* **17**, 35–56 (2018).
4. Puschnik, A. S. et al. A small-molecule oligosaccharyltransferase inhibitor with pan-flaviviral activity. *Cell Rep.* **21**, 3032–3039 (2017).
5. Apte-Sengupta, S., Sirohi, D. & Kuhn, R. J. Coupling of replication and assembly in flaviviruses. *Curr. Opin. Virol.* **9**, 134–142 (2014).
6. Fernandez-Garcia, M. D., Mazzon, M., Jacobs, M. & Amara, A. Pathogenesis of flavivirus infections: using and abusing the host cell. *Cell Host Microbe* **5**, 318–328 (2009).
7. Walsh, D. & Mohr, I. Viral subversion of the host protein synthesis machinery. *Nat. Rev. Microbiol.* **9**, 860–875 (2011).
8. Garcia-Blanco, M. A., Vasudevan, S. G., Bradrick, S. S. & Nicchitta, C. Flavivirus RNA transactions from viral entry to genome replication. *Antivir. Res.* **134**, 244–249 (2016).
9. Chu, C. et al. Systematic discovery of Xist RNA binding proteins. *Cell* **161**, 404–416 (2015).
10. Chen, C. K. et al. Xist recruits the X chromosome to the nuclear lamina to enable chromosome-wide silencing. *Science* **354**, 468–472 (2016).
11. Balinsky, C. A. et al. *IRAV* (*FLJ11286*), an interferon-stimulated gene with antiviral activity against dengue virus, interacts with MOV10. *J. Virol.* **91**, e01606-16 (2017).
12. Paranjape, S. M. & Harris, E. Y box-binding protein-1 binds to the dengue virus 3′-untranslated region and mediates antiviral effects. *J. Biol. Chem.* **282**, 30497–30508 (2007).
13. Umareddy, I. et al. Dengue virus regulates type I interferon signalling in a strain-dependent manner in human cell lines. *J. Gen. Virol.* **89**, 3052–3062 (2008).
14. Lei, Y. et al. Functional interaction between cellular p100 and the dengue virus 3′ UTR. *J. Gen. Virol.* **92**, 796–806 (2011).
15. Hentze, M. W., Castello, A., Schwarzl, T. & Preiss, T. A brave new world of RNA-binding proteins. *Nat. Rev. Mol. Cell Biol.* **19**, 327–341 (2018).
16. Marceau, C. D. et al. Genetic dissection of *Flaviviridae* host factors through genome-scale CRISPR screens. *Nature* **535**, 159–163 (2016).
17. Savidis, G. et al. Identification of Zika virus and dengue virus dependency factors using functional genomics. *Cell Rep.* **16**, 232–246 (2016).
18. Zhang, R. et al. A CRISPR screen defines a signal peptide processing pathway required by flaviviruses. *Nature* **535**, 164–168 (2016).
19. Lin, D. L. et al. Dengue virus hijacks a noncanonical oxidoreductase function of a cellular oligosaccharyltransferase complex. *mBio* **8**, e00939-17 (2017).
20. Li, J.et al. A short hairpin RNA screen of interferon-stimulated genes identifies a novel negative regulator of the cellular antiviral response. *mBio* **4**, e00385-13 (2013).
21. Cui, X. A., Zhang, H. & Palazzo, A. F. p180 promotes the ribosome-independent localization of a subset of mRNA to the endoplasmic reticulum. *PLoS Biol.* **10**, e1001336 (2012).
22. Mobin, M. B. et al. The RNA-binding protein vigilin regulates VLDL secretion through modulation of *Apob* mRNA translation. *Nat. Commun.* **7**, 12848 (2016).
23. Losfeld, M. E., Soncin, F., Ng, B. G., Singec, I. & Freeze, H. H. A sensitive green fluorescent protein biomarker of N-glycosylation site occupancy. *FASEB J.* **26**, 4210–4217 (2012).
24. Reid, D. W. et al. Dengue virus selectively annexes endoplasmic reticulum-associated translation machinery as a strategy for co-opting host cell protein synthesis. *J. Virol.* **92**, e01766-17 (2018).
25. Zarnegar, B. J. et al. irCLIP platform for efficient characterization of protein–RNA interactions. *Nat. Methods* **13**, 489–492 (2016).
26. Savitz, A. J. & Meyer, D. I. Identification of a ribosome receptor in the rough endoplasmic reticulum. *Nature* **346**, 540–544 (1990).
27. Eliseev, B. et al. Structure of a human cap-dependent 48S translation pre-initiation complex. *Nucleic Acids Res.* **46**, 2678–2689 (2018).
28. Belanger, L., Roy, S. & Allard, D. New albumin gene 3′ adjacent to the α_1-fetoprotein locus. *J. Biol. Chem.* **269**, 5481–5484 (1994).
29. Shelness, G. S., Ingram, M. F., Huang, X. F. & DeLozier, J. A. Apolipoprotein B in the rough endoplasmic reticulum: translation, translocation and the initiation of lipoprotein assembly. *J. Nutr.* **129**, 456S–462S (1999).
30. Darnell, J. C. et al. FMRP stalls ribosomal translocation on mRNAs linked to synaptic function and autism. *Cell* **146**, 247–261 (2011).
31. Chen, Y. L., Yokokawa, F. & Shi, P. Y. The search for nucleoside/nucleotide analog inhibitors of dengue virus. *Antivir. Res.* **122**, 12–19 (2015).
32. Cheng, M. H. & Jansen, R. P. A jack of all trades: the RNA-binding protein vigilin. *WIRES RNA* **8**, e1448 (2017).
33. Cui, X. A. & Palazzo, A. F. Localization of mRNAs to the endoplasmic reticulum. *WIRES RNA* **5**, 481–492 (2014).

34. Cunningham, K. S., Dodson, R. E., Nagel, M. A., Shapiro, D. J. & Schoenberg, D. R. Vigilin binding selectively inhibits cleavage of the vitellogenin mRNA 3′-untranslated region by the mRNA endonuclease polysomal ribonuclease 1. *Proc. Natl Acad. Sci. USA* **97**, 12498–12502 (2000).
35. Hyde, M., Block-Alper, L., Felix, J., Webster, P. & Meyer, D. I. Induction of secretory pathway components in yeast is associated with increased stability of their mRNA. *J. Cell Biol.* **156**, 993–1001 (2002).
36. Reid, D. W. & Nicchitta, C. V. Diversity and selectivity in mRNA translation on the endoplasmic reticulum. *Nat. Rev. Mol. Cell Biol.* **16**, 221–231 (2015).
37. Ueno, T., Kaneko, K., Sata, T., Hattori, S. & Ogawa-Goto, K. Regulation of polysome assembly on the endoplasmic reticulum by a coiled-coil protein, p180. *Nucleic Acids Res.* **40**, 3006–3017 (2012).
38. Kruse, C. et al. The multi-KH protein vigilin associates with free and membrane-bound ribosomes. *Cell. Mol. Life Sci.* **60**, 2219–2227 (2003).
39. Batlle, M., Marsellach, F. X., Huertas, D. & Azorin, F. *Drosophila* vigilin, DDP1, localises to the cytoplasm and associates to the rough endoplasmic reticulum. *Biochim. Biophys. Acta* **1809**, 46–55 (2011).
40. Frey, S., Pool, M. & Seedorf, M. Scp160p, an RNA-binding, polysome-associated protein, localizes to the endoplasmic reticulum of *Saccharomyces cerevisiae* in a microtubule-dependent manner. *J. Biol. Chem.* **276**, 15905–15912 (2001).
41. Hirschmann, W. D. et al. Scp160p is required for translational efficiency of codon-optimized mRNAs in yeast. *Nucleic Acids Res.* **42**, 4043–4055 (2014).
42. Phillips, S. L., Soderblom, E. J., Bradrick, S. S. & Garcia-Blanco, M. A. Identification of proteins bound to dengue viral RNA in vivo reveals new host proteins important for virus replication. *mBio* **7**, e01865-15 (2016).
43. Viktorovskaya, O. V., Greco, T. M., Cristea, I. M. & Thompson, S. R. Identification of RNA binding proteins associated with dengue virus RNA in infected cells reveals temporally distinct host factor requirements. *PLoS Negl. Trop. Dis.* **10**, e0004921 (2016).
44. Schoggins, J. W. et al. A diverse range of gene products are effectors of the type I interferon antiviral response. *Nature* **472**, 481–485 (2011).
45. Carette, J. E. et al. Ebola virus entry requires the cholesterol transporter Niemann–Pick C1. *Nature* **477**, 340–343 (2011).
46. Mlera, L., Meade-White, K., Saturday, G., Scott, D. & Bloom, M. E. Modeling Powassan virus infection in *Peromyscus leucopus*, a natural host. *PLoS Negl. Trop. Dis.* **11**, e0005346 (2017).
47. Shan, C. et al. An infectious cDNA clone of Zika virus to study viral virulence, mosquito transmission, and antiviral inhibitors. *Cell Host Microbe* **19**, 891–900 (2016).
48. Lanke, K. H. et al. GBF1, a guanine nucleotide exchange factor for Arf, is crucial for coxsackievirus B3 RNA replication. *J. Virol.* **83**, 11940–11949 (2009).
49. Metsalu, T. & Vilo, J. ClustVis: a web tool for visualizing clustering of multivariate data using Principal Component Analysis and heatmap. *Nucleic Acids Res.* **43**, W566–W570 (2015).
50. Teo, G. et al. SAINTq: scoring protein-protein interactions in affinity purification - mass spectrometry experiments with fragment or peptide intensity data. *Proteomics* **16**, 2238–2245 (2016).
51. Sanjana, N. E., Shalem, O. & Zhang, F. Improved vectors and genome-wide libraries for CRISPR screening. *Nat. Methods* **11**, 783–784 (2014).
52. Li, W. et al. MAGeCK enables robust identification of essential genes from genome-scale CRISPR/Cas9 knockout screens. *Genome Biol.* **15**, 554 (2014).
53. Huang da, W., Sherman, B. T. & Lempicki, R. A. Systematic and integrative analysis of large gene lists using DAVID bioinformatics resources. *Nat. Protoc.* **4**, 44–57 (2009).
54. Carette, J. E. et al. Global gene disruption in human cells to assign genes to phenotypes by deep sequencing. *Nat. Biotechnol.* **29**, 542–546 (2011).

Acknowledgements

We would like to thank A. Rubin, O. Botvinnik, M. R. Corces and A. Za for their helpful discussions on statistical and computational analyses; J. Ule, J. Zmrzlikar and N. Haberman for help with the iCount peak-calling software; L. Zhang and the Elias lab for assistance running samples for mass spectrometry analysis; J. Coller, X. Ji, D. Wagh and the Stanford Functional Genomics Facility for assistance with running samples for deep sequencing. We also thank the Stanford shared FACS facility and its former director M. Bigos for technical assistance. We acknowledge the NIH Biodefense and Emerging Infections Research Repository (BEI Resources) and the NIAID, NIH for providing the multiple DENV and ZIKV strains mentioned in Methods. We thank S. Braun and the members of the Carette, Kirkegaard and Sarnow labs for their helpful discussions and critical reading of the manuscript. The work was funded in part by the NIH (grant nos DP2 AI104557, R01 AI141970 and U19 AI109662 to J.E.C.; R37 AI047365 and R01 AI069000 to P.S. and R01 AI051622 to C.R.B.), the Burroughs Wellcome Investigators in the Pathogenesis of Infectious Disease (J.E.C.), the David and Lucile Packard Foundation (J.E.C.), the Stanford Dean's Fellowship (Y.S.O.), the Child Health Research Institute Stanford (K.M.), the Damon Runyon Cancer Research Foundation (R.A.F.), the NSF-GRF (A.G.J. and C.D.M.) and the Howard Hughes Medical Institute (C.R.B.). C.D.M., J.G., L.M. and M.E.B. were supported by the Intramural Research Program of the NIAID.

Author contributions

Y.S.O., K.M. and R.A.F. were responsible for the design and execution of experiments, data analysis and manuscript preparation. M.A.M. and P.S. performed and analysed the northern blot assays. J.D. carried out the MAGECK analysis for all CRISPR screening results. J.K.L. and N.R. assisted with the proteomic experiments. N.V.B. and K.K. were responsible for the immunofluorescence and fluorescent in situ hybridization targeting assays. A.G.J. assisted with the preparation of manuscript. A.S.P. and C.D.M. helped with the preparation of reagents, cell lines and viruses. L.M., J.M.G. and M.E.B. were responsible for the infection assays and analyses involving POWV. J.E.C. and C.R.B. supervised the research, acquired funding, interpreted data and prepared the manuscript.

Competing interests

The authors declare no competing interests.

Additional information

Supplementary information is available for this paper at https://doi.org/10.1038/s41564-019-0518-2.

Reprints and permissions information is available at www.nature.com/reprints.

Correspondence and requests for materials should be addressed to R.A.F. or J.E.C.

Publisher's note: Springer Nature remains neutral with regard to jurisdictional claims in published maps and institutional affiliations.

nature research

Corresponding author(s): Jan E. Carette, Ryan A. Flynn

Last updated by author(s): Apr 16, 2019

Reporting Summary

Nature Research wishes to improve the reproducibility of the work that we publish. This form provides structure for consistency and transparency in reporting. For further information on Nature Research policies, see Authors & Referees and the Editorial Policy Checklist.

Statistics

For all statistical analyses, confirm that the following items are present in the figure legend, table legend, main text, or Methods section.

n/a	Confirmed	
☐	☒	The exact sample size (*n*) for each experimental group/condition, given as a discrete number and unit of measurement
☐	☒	A statement on whether measurements were taken from distinct samples or whether the same sample was measured repeatedly
☐	☒	The statistical test(s) used AND whether they are one- or two-sided *Only common tests should be described solely by name; describe more complex techniques in the Methods section.*
☐	☒	A description of all covariates tested
☐	☒	A description of any assumptions or corrections, such as tests of normality and adjustment for multiple comparisons
☐	☒	A full description of the statistical parameters including central tendency (e.g. means) or other basic estimates (e.g. regression coefficient) AND variation (e.g. standard deviation) or associated estimates of uncertainty (e.g. confidence intervals)
☒	☐	For null hypothesis testing, the test statistic (e.g. *F*, *t*, *r*) with confidence intervals, effect sizes, degrees of freedom and *P* value noted *Give P values as exact values whenever suitable.*
☒	☐	For Bayesian analysis, information on the choice of priors and Markov chain Monte Carlo settings
☒	☐	For hierarchical and complex designs, identification of the appropriate level for tests and full reporting of outcomes
☐	☒	Estimates of effect sizes (e.g. Cohen's *d*, Pearson's *r*), indicating how they were calculated

Our web collection on statistics for biologists contains articles on many of the points above.

Software and code

Policy information about availability of computer code

Data collection	irCLIP data were collected in biological duplicate and generated on Illumina NextSeq 500 instrument. ChIRP-MS data were collected in biological triplicate and generated on a Thermo Orbitrap Fusion instrument. CRISPR-Cas9 KO screens and Haploid Genetic screens data were generated on Illumina NextSeq 500 instrument.
Data analysis	- MAGeCK (version 0.5.4) (PMID 25476605) was used for CRISPR-Cas9 screen analyses. - Deep sequencing data from Haploid Genetic Screen was analyzed as previously described (PMID: 27383987). - ImageJ colocalization algorithm COLOC2 (https://github.com/fiji/Colocalisation_Analysis/releases/tag/Colocalisation_Analysis-3.0.0) was used to quantify colocalization between proteins and/or viral RNAs. - SAINTq software (http://saint-apms.sourceforge.net/Main.html) was used to apply a statistical confidence filter to refine the ChIRP-MS hits - The Database for Annotation, Visualization and Integrated Discovery, DAVID (https://david.ncifcrf.gov/tools.jsp) was used for gene ontology (GO) analysis. - irCLIP data were analyzed using a custom script available at: https://github.com/ChangLab/FAST-iCLIP/tree/lite.

For manuscripts utilizing custom algorithms or software that are central to the research but not yet described in published literature, software must be made available to editors/reviewers. We strongly encourage code deposition in a community repository (e.g. GitHub). See the Nature Research guidelines for submitting code & software for further information.

Data

Policy information about availability of data

All manuscripts must include a data availability statement. This statement should provide the following information, where applicable:

- Accession codes, unique identifiers, or web links for publicly available datasets
- A list of figures that have associated raw data
- A description of any restrictions on data availability

Raw and processed sequencing data will be deposited on GEO: GSE109194

Field-specific reporting

Please select the one below that is the best fit for your research. If you are not sure, read the appropriate sections before making your selection.

☒ Life sciences ☐ Behavioural & social sciences ☐ Ecological, evolutionary & environmental sciences

For a reference copy of the document with all sections, see nature.com/documents/nr-reporting-summary-flat.pdf

Life sciences study design

All studies must disclose on these points even when the disclosure is negative.

Sample size	For each experimental type, an appropriate number of data points or experiments were collected. For example, deep sequencing experiments were performed in duplicate, while qRT-PCR experiments were performed in at least triplicate.
Data exclusions	No relevant data were excluded.
Replication	As no data were excluded, all values from each experiment are presented and the variation can be seen in the figures. Statistical analysis as described throughout the manuscript provided the ability to confidently assess differences between different experimental conditions.
Randomization	No randomization was used.
Blinding	No blinding was used.

Reporting for specific materials, systems and methods

We require information from authors about some types of materials, experimental systems and methods used in many studies. Here, indicate whether each material, system or method listed is relevant to your study. If you are not sure if a list item applies to your research, read the appropriate section before selecting a response.

Materials & experimental systems

n/a	Involved in the study
☐	☒ Antibodies
☐	☒ Eukaryotic cell lines
☒	☐ Palaeontology
☒	☐ Animals and other organisms
☒	☐ Human research participants
☒	☐ Clinical data

Methods

n/a	Involved in the study
☒	☐ ChIP-seq
☒	☐ Flow cytometry
☒	☐ MRI-based neuroimaging

Antibodies

Antibodies used

Mouse anti-GAPDH, GeneTex, catalog # GTX627408
Mouse anti-P84, GeneTex, catalog # GTX70220
Rabbit anti-DENV prM, GeneTex, catalog #GTX128092
Rabbit anti-DENV NS3, GeneTex, catalog #GTX124252
Rabbit anti-RRBP1, Bethyl Laboratories, catalog # A303-996A
Rabbit anti-Vigilin, Bethyl Laboratories, catalog # A303-971A
Rabbit anti-RPN1, Bethyl Laboratories, catalog # A305-026A
Rabbit anti-beta tubulin, Abcam, catalog #ab97872
IgG, Thermo Fisher Scientific, catalog # 02-6102
Mouse GFP tag antibody, Thermo Fisher Scientific, catalog # MA5-15256
Goat anti-mouse IgG (HRP), GeneTex, catalog # GTX213111-01
Goat anti-rabbit IgG (HRP), GeneTex, catalog # GTX213110-01
Alexa Fluor 488nm, Thermo Fisher Scientific, catalog # A11034

Alexa Fluor 594nm, Thermo Fisher Scientific, catalog # R37117
Alexa Fluor 647nm, Thermo Fisher Scientific, catalog # A31573

Validation

Antibody validation was accomplished by the provider.

Eukaryotic cell lines

Policy information about cell lines

Cell line source(s)

American Type Culture Collection (ATCC): H1-HeLa (CRL-1968), rhabdomyosarcoma (RD) (CCL-136), Vero cells (CCL-81), C6/36 cells (CRL-1660).Thermo Fisher Scientific: 293FT (R70007). Huh7.5.1 was provided by Frank Chisari Lab. HAP1 cells was originally generated by Jan Carette and Thijn Brummelkamp (PMID: 21866103). BHK-21 cells was provided by Karla Kirkegaard lab.

Authentication

Authentication was accomplished by the provider.

Mycoplasma contamination

All cell lines tested negative for mycoplasma contamination.

Commonly misidentified lines
(See ICLAC register)

N/A